recycling

MDPI

Article

A Comparative Evaluation of Three Valorisation Pathways for Waste Electric Arc Furnace Slag to Improve Its Use as an Eco-Logical Binder

Bruno Machini [1,2], Diogo Simões [3], Pedro Humbert [4], Julieta António [1,5] and João Almeida [1,2,*]

[1] Itecons—Institute for Research and Technological Development in Construction, Energy Environment and Sustainability, Rua Pedro Hispano, 3030-289 Coimbra, Portugal; bruno.machini@itecons.uc.pt (B.M.); julieta@dec.uc.pt (J.A.)
[2] CERIS, University of Coimbra, Rua Luís Reis Santos, Pólo II, 3030-790 Coimbra, Portugal
[3] Department of Civil Engineering, University of Coimbra, Rua Luís Reis Santos, Pólo II, 3030-790 Coimbra, Portugal
[4] Innovation Centre for Sustainable Construction, CRH, De Klencke 10, 1083 HL Amsterdam, The Netherlands; phumbert@crh.com
[5] CERIS, Department of Civil Engineering, University of Coimbra, Rua Luís Reis Santos, Pólo II, 3030-790 Coimbra, Portugal
* Correspondence: joao.almeida@itecons.uc.pt

Abstract

The urgent need to reduce greenhouse gas emissions and enhance resource circularity is driving the cement and construction industry to explore alternatives to clinker-based binders. Electric arc furnace slag (EAFS), a major steelmaking by-product, is currently underutilised as a binder due to its low intrinsic reactivity. This study provides a comparative evaluation of three distinct valorisation pathways for the same EAFS—use as a supplementary cementitious material (SCM), as a precursor for alkali-activated binders, and as a component in accelerated carbonation systems—thereby highlighting its multifunctional and more ecological binding potential. A comprehensive physicochemical characterisation was conducted, followed by mechanical performance assessment under different curing regimes. When used as an SCM, partial cement replacement resulted in no loss of mechanical performance and a compressive strength increase of up to 8.9% at 10% replacement, demonstrating its suitability for structural applications. Under accelerated carbonation, specimens with 50% replacement of cement and sand achieved compressive strengths of 46.7 MPa, comparable to the non-carbonated reference (47 MPa), indicating full strength recovery despite high substitution levels. Full replacement systems based on alkali activation or carbonation of EAFS achieved moderate compressive strengths (~10 MPa), suitable for non-structural applications, with clear potential for improvement through optimisation of activation and curing conditions. Overall, this work demonstrates that EAFS can be effectively valorised through multiple reaction routes, supporting its role as a versatile and low-carbon resource for sustainable cementitious materials.

Keywords: supplementary cementitious materials; alkali-activation; accelerated carbonation; alternative binders; circular economy

Check for updates

Academic Editor: Michele John

Received: 30 December 2025
Revised: 23 January 2026
Accepted: 28 January 2026
Published: 1 February 2026

Copyright: © 2026 by the authors. Licensee MDPI, Basel, Switzerland. This article is an open access article distributed under the terms and conditions of the Creative Commons Attribution (CC BY) license.

1. Introduction

The increasing global population has led to a growing demand for infrastructure, resulting in the extensive use of natural resources and the generation of significant waste.

These factors contribute, either directly or indirectly, to environmental degradation, resource depletion, and climate change [1].

The construction sector is a key contributor to this process, significantly impacting global energy and natural resources use, as well as producing substantial waste and realising greenhouse gases into the atmosphere [2,3]. Only the Portland cement manufacturing, which is recognized as fundamental to this sector and indispensable for social and economic reasons, contributes up to 8% of world anthropogenic CO_2 emissions [4,5].

To address these global challenges, various targets and commitments have been established to reduce greenhouse gas emissions and enhance resource circularity [6–8]. Among the potential approaches to improve the environmental efficiency of the cement and concrete industry, the development of more ecological binders that can partially or entirely substitute clinker, and that are produced from waste or by-products, stands out [9].

Given its abundance, the residues and co-products generated by the steel industry are of significant interest. As reported by the World Steel Association [10], producing one tonne of steel generates approximately 400 kg of co-products in the blast furnace-basic oxygen furnace (BF-BOF) and 200 kg for the electric arc furnace (EAF) process. The predominant solid co-product formed during the iron and crude steel production is slag (accounting for about 90% by weight), followed by dust and sludge. Alongside these, gaseous co-products are also formed, such as carbon monoxide, carbon dioxide, and methane.

Over the last decades, the use of these co-products has increased significantly thanks to innovative technological developments and synergies with other industries, getting ever closer to the goal of zero waste to landfills [11]. Some applications of co-products from the steel industry can be highlighted, such as blast furnace slag as substituent for Portland cement [12], steel slag for clinker production [13,14], both blast furnace and steel slags in road construction [15–18], asphalt concrete [19–21], agricultural fertiliser [22–25], and soil improvement [26,27], as well as dust and sludge for recovery of metals [28,29] and gases for heat and electricity production [30].

In recent years, research on slag-based cementitious materials has increasingly focused on enhancing their performance and broadening their applicability through different development strategies. These include the physical and chemical modification of slags to improve reactivity and compatibility with cementitious systems [31–34], the development of alternative low-clinker and clinker-free binders, such as alkali-activated materials and geopolymers, to reduce the environmental footprint of conventional cement [35–37], and the assessment of durability-related properties to ensure long-term performance under aggressive exposure conditions [38,39].

As a co-product generated during the steel production process, EAFS is specifically formed after the melting phase and the initial acid refining of liquid steel. Its composition is primarily based on calcium, iron, and silicon oxides and minorly by aluminium, magnesium, manganese, and other oxides. Because of its low reactivity, EAFS has been mostly applied as an alternative to natural coarse and/or fine aggregates in Portland cementitious materials [40–44]. For example, in ultra-high-performance concrete (UHPC) systems, which represent a technologically advanced and increasingly commercialised segment of the construction market due to their superior mechanical performance and durability, EAFS has been primarily employed as a partial or total replacement of natural fine aggregates [45–47].

Recent studies report that the incorporation of EAFS in UHPC can enhance fresh-state properties, particularly flowability, owing to the favourable morphology of slag particles, while maintaining comparable compressive strength levels depending on the replacement ratio and mix design. These investigations underline UHPC as a practically relevant and increasingly mature valorisation pathway for EAFS; however, they predominantly rely

on the optimisation of physical and granular characteristics rather than on the activation of the intrinsic chemical reactivity of the slag [48,49]. In this broader context, alternative waste-to-value approaches can be pursued to enhance the reactive potential and expand the range of applications of EAFS, including its use as a supplementary cementitious material (SCM), alkali activation (AA), and accelerated carbonation (AC) curing.

In general terms, supplementary cementitious materials are fine materials containing soluble and reactive siliceous, aluminosiliceous, or calcium aluminosiliceous compounds, which can partially substitute clinker in cements or Portland cement in concrete mixtures [50]. The alkali-activation is a process characterised by a complex and multi-chain reaction, where a solid aluminosilicate precursor reacts with an alkaline activator, at room temperature, leading to the formation of a hardened product [51]. Finally, the accelerated carbonation can be described as a fast process under an enriched CO_2 atmosphere and specific temperature, humidity, and pressure conditions, promoting the formation of stable carbonates in a short period of time and enhancing early strength development [52].

In this context, this study aimed to investigate the reaction potential of an EAFS with unknown properties, using different alternative waste-to-value approaches, to produce more ecological binders. For this, a systematic physicochemical characterisation of this EAFS, including leaching behaviour, chemical and mineralogical composition, pozzolanic activity, and its effect on cement hydration heat, was conducted. Additionally, different technological strategies (e.g., SCM, AA, and AC) were explored for the EAFS valorisation. The mechanical effects of the EAFS incorporation were assessed by means of compression and flexural strength tests at different curing ages. The innovative character of the work resides in the demonstration of the multifunctional binding potential of EAFS, highlighting how its chemical and mineralogical composition can be mobilised under different activation mechanisms (hydration, alkali activation, and carbonation).

2. Results and Discussion

2.1. Physicochemical Characterisation of the Raw Materials

2.1.1. Physical Properties

The EAFS, in its original state and ground, was characterised in terms of particle size distribution. In addition, the EAFS and S0/4 were characterised in terms of loose bulk density, voids, particle density, water absorption, and moisture content. The particle size distribution curve is presented in Figure 1, while the other physical properties are summarized in Table 1.

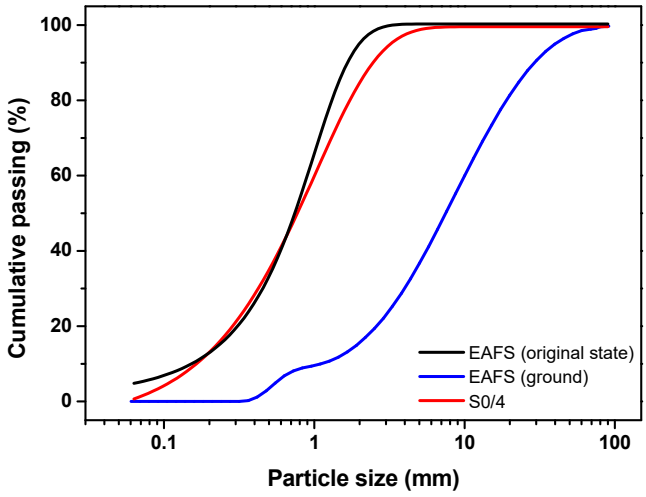


Figure 1. Particle size distribution of the EAFS in its original state (black line), ground (blue line), and S0/4 (red line).

Table 1. Physical properties of the EAFS, in its original state, and S0/4.

Properties	EAFS	S0/4
Loose bulk density (g/cm^3) [EN 1097-3]	1.76	1.51
Voids (%) [EN 1097-3]	34.57	42.80
Particle density (g/cm^3) [EN 1097-6]	3.72	2.65
24 h water absorption (%) [EN 1097-6]	10.2	0.1

2.1.2. Chemical Composition

XRF analyses were performed to determine the chemical composition of EAFS, CEM-II 42.5, and S0/4. The chemical composition of slag varies based on the raw materials used, the manufacturing processes, and the specific operating conditions of the furnace [53]. For the EAFS studied here, a significant content of iron, calcium, and silicon oxides, which together comprise about 77% content, was observed. Other minor contents of aluminium, manganese, and magnesium oxides were also observed. The high content of CaO and MgO in the EAFS can be explained by the use of fluxes in order to minimize impurities, while iron oxides can be attributed to unrecovered iron residues during the conversion of cast iron into steel [54]. For CEM-II 42.5, a significant content of calcium and silicon oxides, followed by a moderate content of aluminium, iron, sulphur, and magnesium oxides, was obtained. For S0/4, a significant content of silicon and aluminium oxides was observed. The full chemical composition of the raw materials is presented in Table 2.

Table 2. Chemical composition (wt.%) of EAFS, CEM-II 42.5, and S0/4 expressed in oxide form.

Parameter	EAFS	CEM-II 42.5	S0/4
Na_2O	0.17	–	–
MgO	5.50	1.31	0.14
Al_2O_3	9.69	3.52	13.9
SiO_2	16.5	14.7	82.2
P_2O_5	0.33	0.14	–
SO_3	0.24	2.40	0.06
Cl	–	0.03	0.02
K_2O	–	0.85	2.40
CaO	30.1	51.5	0.74
TiO_2	0.72	0.33	–
MnO	5.67	–	–
Fe_2O_3	30.4	3.09	0.32
BaO	0.24	–	–
Others	–	0.23	0.01
LOI	–	21.9	0.27

The chemical composition of EAFS and cement were compared, and with the exception of the high content of iron and manganese oxide, which are characteristic of EAFS and its production process, significant contents of calcium, silicon, aluminium, and magnesium oxides were revealed for both materials, suggesting a good correlation between their chemical compositions, and that, in case of replacement of the cement, the EAFS can complement and/or replace the removed chemical compounds.

2.1.3. Mineralogical Phases

XRD analyses were performed to assess the crystalline mineralogical phases of EAFS and CEM-II 42.5. As can be seen in Figure 2, the major mineral phases in EAFS include wüstite (FeO—ICDD 00-006-0615), calcium magnesium silicate ($Ca_5MgSi_3O_{12}$—ICDD 00-034-1350), calcium silicate (Ca_3SiO_5—ICDD 00-049-0442), magnetite (Fe_3O_4—ICDD 01-

075-1610), and gehlenite ($Ca_2Al(AlSiO_7)$—ICDD 01-077-1113). According to the literature, several mineral forms can occur in EAFS, such as dicalcium silicate, merwinite, gehlenite, iron oxides such as wüstite, hematite, and magnetite, mayenite, brownmillerite, and periclase [40].

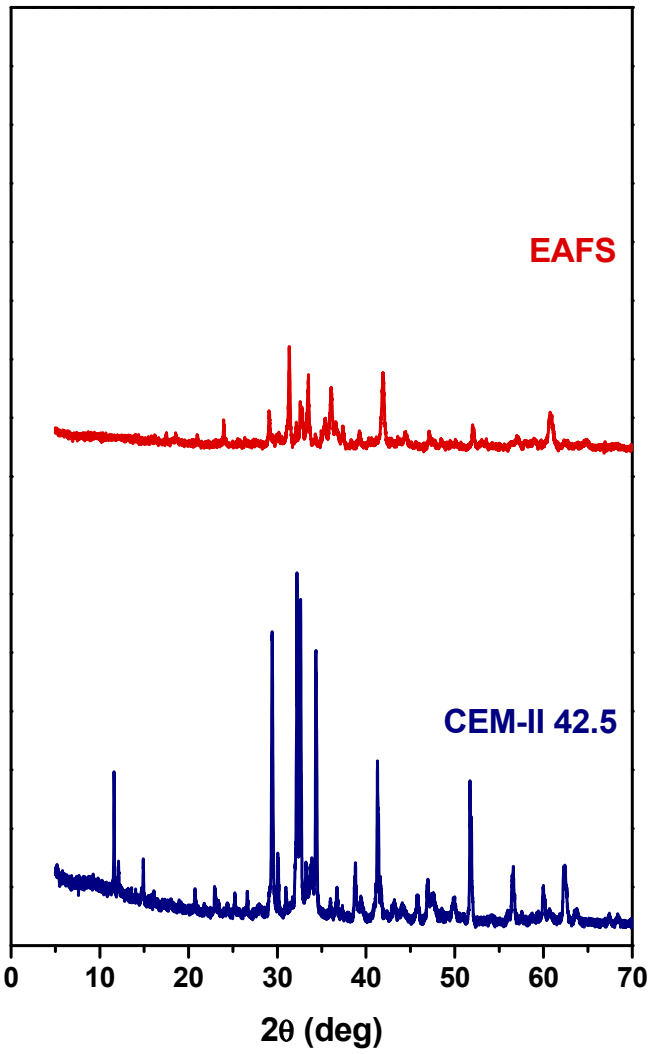


Figure 2. XRD powder patterns of EAFS (top) and CEM-II 42.5 (bottom).

For CEM-II 42.5, the major mineral phases include hatrurite (Ca_3SiO_5—ICDD 01-086-0402), larnite (Ca_2SiO_4—ICDD 01-083-0460), quartz (SiO_2—ICDD 01-083-2465), gypsum ($Ca(SO_4)(H_2O)_2$—ICDD 01-074-1433), brownmillerite ($Ca_2(Al,Fe)_2O_5$—ICDD 00-030-0226), and tricalcium aluminate ($Ca_3Al_2O_6$—ICDD 00-038-1429).

Although these phases are not clearly identifiable in the presented diffractograms, steel slags may contain reactive constituents such as free lime (f-CaO) and free magnesia (f-MgO), which are known to raise durability concerns. The incorporation of steel slag into cementitious systems can be associated with volumetric instability, as the hydration of these compounds may induce expansion [55]. In particular, the hydration of f-CaO has been reported to cause measurable increases in concrete volume [56]. Moreover, delayed expansion related to f-MgO hydration, as well as cracking resulting from the oxidation of residual metallic phases, has been identified as a potential source of long-term durability issues [57].

2.1.4. Leaching Behaviour

Assessing the release of dangerous substances from the EAFS is very important since it may contain potentially toxic chemicals and, consequently, their leachable quantity may affect the environment or human health. Metals such as chromium (Cr), lead (Pb), mercury (Hg), molybdenum (Mo), and cadmium (Cd) have attracted special concern regarding their potential occurrence in EAFS due to their high toxicity to humans as well as to natural ecosystems [58].

Still, about the amount of these substances, the chromium content in the EAFS is considered important and requires additional attention. The Directive 2003/53/EC [59], which was later incorporated into the Regulation EC 1907/2006 [60] of the Registration, Evaluation, Authorisation and Restriction of Chemicals (REACH), establishes that cement and cement-containing preparations shall not be used or placed on the market, if they contain, when hydrated, more than 2 ppm soluble Cr(VI) of the total dry weight of the cement, which could be a real limitation in the use of the EAFS in clinker kilns or even in the partial replacement of cement by slag.

In this context, aqueous extracts of the EAFS were produced following the EN 12457-2 [61] to evaluate the leaching potential of its substances. These extracts were then chemically analysed using the procedures and criteria defined for the waste acceptance at landfills, originally established by the EU Council Decision 2003/33/EC [62] and later transposed into the law of the various European Member States. Total content of organic parameters was also directly analysed in organic extracts produced from the EAFS and respective results compared with the same referential. Table 3 summarizes the results obtained, the limit of quantification (LOQ) of the analytical methods (the smallest concentration of a substance that is possible to be determined by means of the respective analytical method) and the maximum values for the acceptance of waste in landfills for inert waste according to EU Council Decision 2003/33/EC [62] and later transposed into the law of the various European Member States.

Table 3. Leaching and total content of organic parameters results for EAFS according to EN 12457-2 [61].

Parameter (Unit)	EAFS	LOQ [1]	Maximum Value [2]
pH (25 °C)	10.1	---	---
Electric cond. (25 °C, mS/cm)	0.119	---	---
Chloride (mg/kg)	<LOQ	40	800
Fluoride (mg/kg)	10	4	10
Sulphate (mg/kg)	64	40	1000
Phenol index (mg/kg)	<LOQ	0.5	1
TDS (mg/kg)	1070	1000	4000
As (mg/kg)	<LOQ	0.1	0.5
Ba (mg/kg)	<LOQ	5.0	20
Cd (mg/kg)	<LOQ	0.01	0.04
Cr (mg/kg)	<LOQ	0.2	0.5
Cu (mg/kg)	<LOQ	0.4	2
Hg (mg/kg)	<LOQ	0.01	0.01
Mo (mg/kg)	<LOQ	0.2	0.5
Ni (mg/kg)	<LOQ	0.1	0.4
Pb (mg/kg)	<LOQ	0.1	0.5
Sb (mg/kg)	<LOQ	0.02	0.06
Se (mg/kg)	<LOQ	0.02	0.1
Zn (mg/kg)	<LOQ	0.2	4
DOC [3] (mg/kg)	<LOQ	250	500

Table 3. *Cont.*

Parameter (Unit)	EAFS	LOQ [1]	Maximum Value [2]
	Total content		
TOC [4] (mg/kg)	<LOQ	250	30,000
Mineral Oil C10–C40 (mg/kg)	<LOQ	100	500
BTEX [5] (mg/kg)	<LOQ	0.1	6
PCB [6] (mg/kg)	<LOQ	0.5	1
PAH [7] (mg/kg)	<LOQ	10	100

[1] LOQ—Limit of quantification of the analytical method; [2] Maximum values—Maximum values for the acceptance of waste in landfills for inert waste according to EU Council Decision 2003/33/EC and later transposed into the law of the various European Member States; [3] DOC—Dissolved organic carbon; [4] TOC—Total organic carbon; [5] BTEX—Benzene, toluene, ethylbenzene, m-Xylene, p-Xylene, o-Xylene; [6] PCB—PCB 28, PCB 52, PCB 101, PCB 118, PCB 138, PCB 153, PCB 180; [7] PAH—Acenaphthene, acenaphthylene, anthracene, benzo(a)anthracene, benzo(a)pyrene, benzo(b)fluoranthene, benzo(g,h,i)perylene, benzo(k)fluoranthene, chrysene, dibenzo(a,h)anthracene, phenanthrene, fluoranthene, fluorene, indene(1,2,3-cd)pyrene, naphthalene, pyrene.

Rai et al. investigated the leaching behaviour of EAFS from a steelwork manufacturer in India, applying different leaching methods, conditions, duration, and leachates pH [58]. Their findings indicated that the release of hazardous heavy metals from EAFS is negligible or within permissible limits.

Likewise, in our work, most of the parameters surveyed were negligible since the results obtained were lower than LOQ and none of them is above the acceptance limits of inert landfills sites. Note that no heavy metals, organic compounds, and/or mineral oils were quantified, allowing the EAFS under study to be safely utilized in the production of construction materials.

Note that radiological characterisation and compliance with Council Directive 2013/59/EURATOM [63] were not addressed in this study, as the experimental programme focused exclusively on chemical release behaviour; radiometric assessments are typically conducted at later stages of material qualification when the intended construction application is defined.

2.1.5. Pozzolanic Activity

The pozzolanic activity of the EAFS was determined by an adapted procedure based on the Frattini test outlined in EN 196-5 [64]. For each sample, the Ca^{2+} concentration, expressed in terms of CaO, is plotted against the OH^- concentration in Figure 3. Additionally, for assessment purposes, the theoretical maximum CaO concentration was estimated following the methodology outlined in EN 196-5 [64] and used to construct the lime solubility curve. The results obtained below this curve indicate pozzolanic activity, whereas the results above the curve indicate the absence of pozzolanic activity.

According to the results, at 8 and 15 days, EAFS and CEM-II 42.5 are positioned above the solubility line, which corresponds to no pozzolanic activity, while MK (used as a positive control) falls below the solubility line, corroborating its pozzolanic properties, as expected. In terms of the progress of pozzolanic reaction, no significant changes were observed for any of the materials.

The results were further analysed based on the deviation of data points from the CaO solubility curve along the vertical axis at the specific $[OH^-]$. Table 4 shows Frattini test results for the test materials at 8 and 15 days, determined following to EN 196-5 [64], along with the percentage of the theoretical maximum removed for the materials at 8 and 15 days. Note that for those materials with a calculated theoretical maximum CaO lower than the measured CaO, it was not possible to calculate CaO reduction [65,66].

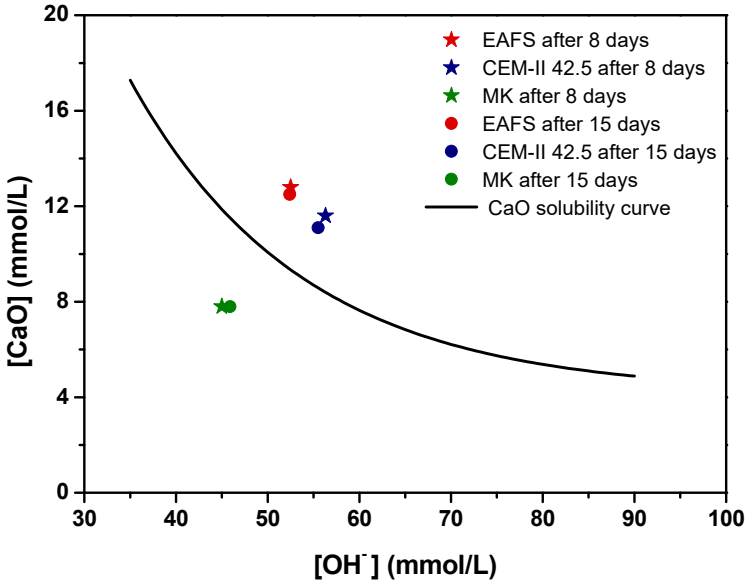


Figure 3. Pozzolanic activity for EAFS (red), CEM-II 42.5 (blue), and MK (green) after 8 (★) and 15 (●) days, assessed by an adapted procedure based on the Frattini test.

Table 4. Eight and fifteen days Frattini test results for the test materials quantified according to EN 196-5 [64].

Material	8 Days				15 Days			
	[OH⁻] mmol/L	[CaO] mmol/L	Theoretical Max. [CaO] mmol/L	[CaO] reduction %	[OH⁻] mmol/L	[CaO] mmol/L	Theoretical Max. [CaO] mmol/L	[CaO] Reduction %
EAFS	52.5	12.8	9.3	–	52.4	12.5	9.4	–
CEM-II 42.5	56.3	11.6	8.5	–	55.5	11.1	8.6	–
MK	45.0	7.8	11.7	33.3	45.9	7.8	11.3	31.0

This analysis reveals larger amounts of CaO in solution than expected, in relation to the theoretical maximum [CaO] values, for EAFS and cement. In contrast, for MK (positive control), lime removal was calculated to be approximately 33% after 8 days and 31% after 15 days, showing its high pozzolanic activity.

2.1.6. Hydration Heat

Isothermal calorimetry was conducted to evaluate the effect of EAFS incorporation on the cement hydration heat, both in terms of extent and kinetics. The monitored heat flow and the calculated cumulative heat of the cementitious pastes with different percentages of EAFS are shown in Figure 4.

According to the results, a large exothermic signal (peak I) attributed to the initial dissolution of cement particles [67] was observed, suggesting that, at this stage, the reaction occurs rapidly, within the first 1–2 min. The second and third peaks (peak II and peak III) can be attributed to the hydration of C_3S and C_3A [68], respectively, suggesting that the initial reactions occurred within the first 8 h, for all cement-EAFS pastes analysed, including the cement control paste. For the cement-EAFS pastes, a slight change in curve profile was observed, specifically a decrease in the intensity of peak II accompanied by an enhancement in peak III. This fact can be attributed to the slag hydration [69], suggesting that the EAFS incorporation contributes more effectively to promote the hydration reaction of C_3A.

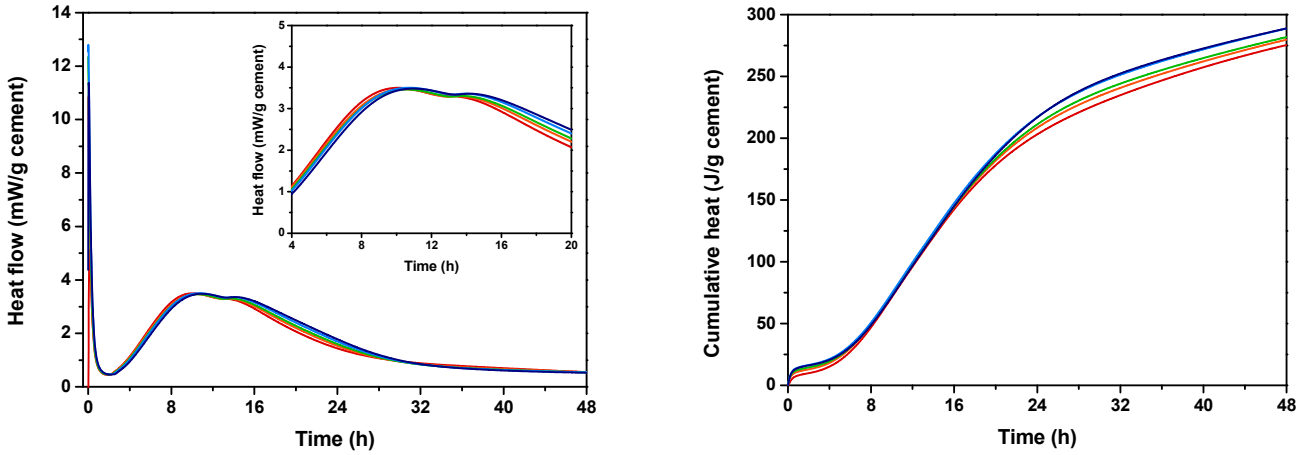


Figure 4. Hydration heat flow rate (**a**) and cumulative hydration heat (**b**) for cement control (red) and cement pastes incorporating 5% (orange), 10% (green), 15% (blue), and 20% (navy) EAFS.

The setting behaviour corresponds to the transition period between the fluidity and rigidity stages of the pastes, and it is controlled by the development of the three-dimensional microstructure of the blended binders. This process involves multiple phenomena, including the formation of new phases, particle nucleation, structural percolation, and interconnection of cement hydration products [70]. Given that these phenomena are closely linked to the cement hydration process, which is reflected in its heat release profile, the setting time of the pastes can be estimated by evaluating the heat evolution curve [70].

Considering that, it was possible to observe that the setting time prolonged, as well as the amount of heat released after 48 h increased with the incorporation of EAFS. The setting time increased from 10.03 h for the cement control paste to 10.42 h up to 11.04 h for the cement-EAFS pastes containing 5% and 20% EAFS, which corresponds to an increase between 3.89% and 10.07%. Also, the hydration heat after 48 h increased from 276.3 J/g cement for the cement control paste to 294.2 J/g cement up to 361.1 J/g cement for the cement-EAFS pastes containing 5% and 20% EAFS, which corresponds to an increase between 6.48% and 30.69% compared to the control cement paste.

In this way, the presence of EAFS affects the hydration kinetics, leading to a delay in cement hydration and contributing to a noticeable increase in heat production. The results obtained for the different percentages of EAFS incorporation are summarised in Table 5.

Table 5. Setting time and hydration heat after 48 h for the cement control and cement-EAFS pastes.

Sample Reference	Setting Time (h)	Setting Time Delay Relative to the Control (h)	Hydration Heat (J/g Cement)	Hydration Heat Variation Relative to the Control (%)
CEM-II 42.5 (control)	10.03	–	276.3	–
CEM-II 42.5 + 5% EAFS	10.42	0.39	294.3	6.48
CEM-II 42.5 + 10% EAFS	10.71	0.68	313.0	13.28
CEM-II 42.5 + 15% EAFS	10.76	0.73	339.6	22.91
CEM-II 42.5 + 20% EAFS	11.04	1.01	361.1	30.69

2.2. Mechanical and Mineralogical Characterisation

In order to investigate the effect of the EAFS incorporation on the mechanical properties of the hardened materials resulting from the different valorisation approaches, test specimens were prepared as previously described and subjected to mechanical and min-

eralogical characterisation tests at 7 and 28 days. The results obtained are presented and discussed in the next subsections.

2.2.1. Supplementary Cementitious Materials

The compressive and flexural strength results for the cement (control) and cement-EAFS specimens after 7 and 28 days are presented in Figure 5. This graphical representation clearly illustrates that the compressive strength of the cement-EAFS specimens is influenced by EAFS in a nonmonotonic manner. Notably, the specimens incorporating 10% EAFS exhibited a strength increase of 12.4% and 8.9% after 7 and 28 days, respectively, which resulted in the highest strength values attained. This increase in compressive strength can be attributed to the formation of hydration products, mainly C–S–H, which contribute to pore refinement within the hardened material.

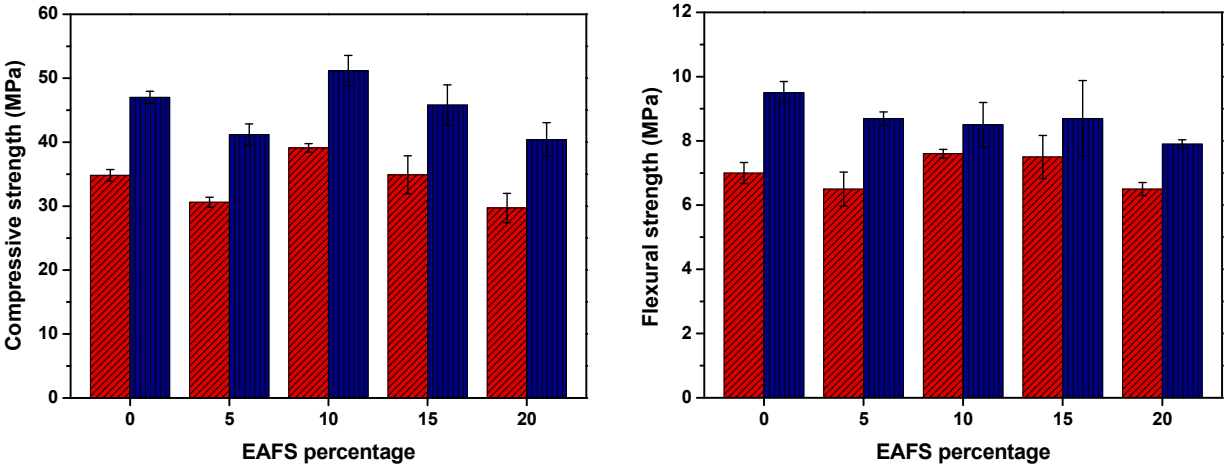


Figure 5. Compressive (n = 6) (**a**) and flexural (n = 3) (**b**) strength (mean values ± standard deviation) for the cement control and cement-EAFS specimens at 7 days (red) and 28 days (blue).

Although no pozzolanic activity was observed from the EAFS particles under the conditions of the Frattini test, the presence of mineralogical phases, which may serve as a reagent source for limiting components of the cement hydration reactions, and filler effects that may lead to a decrease in the total porosity of the hardened material may be related to the role of EAFS as a partial substituent of cement. Ramadan et al. reported similar effects in the strength development of blended cement pastes containing an EAFS from a flat steel company in Egypt. In that study, the partial replacement of cement by 6% EAFS caused an improvement in compressive strength compared to the control specimen [71].

Conversely, for the remaining specimens containing 5%, 15%, and 20% EAFS, it is possible to observe a reduction in the compressive strength compared to the respective cement control specimens, which suggests that for nonoptimal percentages of EAFS, disruptive effects caused in the cement matrix by nonreactive mineralogical phases or excess of unreacted phases may exceed the benefits previously described related with the introduction of small amounts of reactive forms and filler effects. Despite this, all specimens revealed a compressive strength exceeding 40 MPa after 28 days, which is a relatively small drop when compared with the control specimens containing only cement (47 MPa).

The flexural strength results for the cement-EAFS specimens after 7 days exhibited a similar behaviour to compressive strength, with a significant increase on the flexural strength of above 7% for the specimens containing 10% and 15% EAFS. On the other hand, the results for the cement-EAFS specimens after 28 days show a reduction on the flexural strength for all the EAFS incorporation percentages (between 8.4% and 16.8%). In this case,

disruptive effects caused in the cement matrix by nonreactive mineralogical phases present in EAFS may exceed the small reactivity effect of this incorporation, even for the optimal composition previously observed in the compressive tests. Despite this, all specimens revealed a flexural strength greater than 8 MPa after 28 days, which is a relatively small drop when compared with the control specimens containing only cement (9.5 MPa).

The compressive and flexural strength results for the cement control and cement-EAFS specimens at 7 and 28 days are summarized in Table 6.

Table 6. Compressive (n = 6) and flexural (n = 3) strength (mean ± standard deviation) for the cement control and cement-EAFS specimens at 7 and 28 days.

Sample Reference	Compressive Strength (MPa)		Flexural Strength (MPa)	
	7 Days	28 Days	7 Days	28 Days
SCM-0% EAFS (control)	34.8 ± 0.92	47.0 ± 0.93	7.00 ± 0.33	9.50 ± 0.35
SCM-5% EAFS	30.6 ± 0.79	41.2 ± 1.63	6.50 ± 0.53	8.70 ± 0.20
SCM-10% EAFS	39.1 ± 0.68	51.2 ± 2.37	7.60 ± 0.13	8.50 ± 0.69
SCM-15% EAFS	34.9 ± 2.96	45.8 ± 3.16	7.50 ± 0.67	8.70 ± 1.18
SCM-20% EAFS	29.7 ± 2.30	40.4 ± 2.64	6.50 ± 0.20	7.90 ± 0.13

In order to identify the reaction products, powder X-ray diffraction tests were performed on cement and cement-EAFS pastes (without sand). The diffractograms presented in Figure 6 reveal subtle variations between the patterns, suggesting that the main crystalline phases are the same, regardless of the presence of the EAFS and the percentage of replacement of cement by EAFS. Among the phases detected, there are several products characteristic of hydrated cement (e.g., portlandite, ettringite, gypsum, etc.), in addition to tricalcium silicate (C_3S), the main component of cement. The fact that, in most pastes, it was not possible to observe crystalline phases characteristic of the EAFS (e.g., gehlenite and wüstite) suggests that there was a dissolution of them during the cement hydration process. Only in pastes containing a higher percentage of EAFS (i.e., 20%) is it possible to observe traces of phases characteristic of EAFS (e.g., gehlenite), which can be attributed to an excess of unreacted EAFS. These results support the proposed mechanism mentioned above, indicating that EAFS can act as a reagent source for limiting components of the cement hydration reactions. An effect that may compete with other disruptive effects caused in the cement matrix by the presence of nonreactive phases introduced by EAFS particles.

Additionally, the higher intensity of the peaks observed in the pastes containing 10% EAFS may indicate an optimal stoichiometric balance between the amount of cement and EAFS, which corroborates the greater compressive strength found for this mixture. The greater compressive strength can also be explained by the formation of new amorphous phases [72], namely calcium silicate hydrate (C–S–H), not detected by this technique. Note that the greater heat release in the cement hydration process with the incorporation of EAFS, observed with the isothermal calorimetry results, suggests that the extension of the cement hydration reaction is greater in the presence of EAFS. This is probably due to the reaction between the cement and the EAFS.

2.2.2. Alkali Activation

The compressive and flexural strength results for the alkali-activated EAFS composites after 7 and 28 days are presented in Figure 7. Although three mixtures were prepared, it was not possible to obtain results for a control sample without alkaline activator since it did not show binding properties, resulting in its breakdown during the demoulding process.

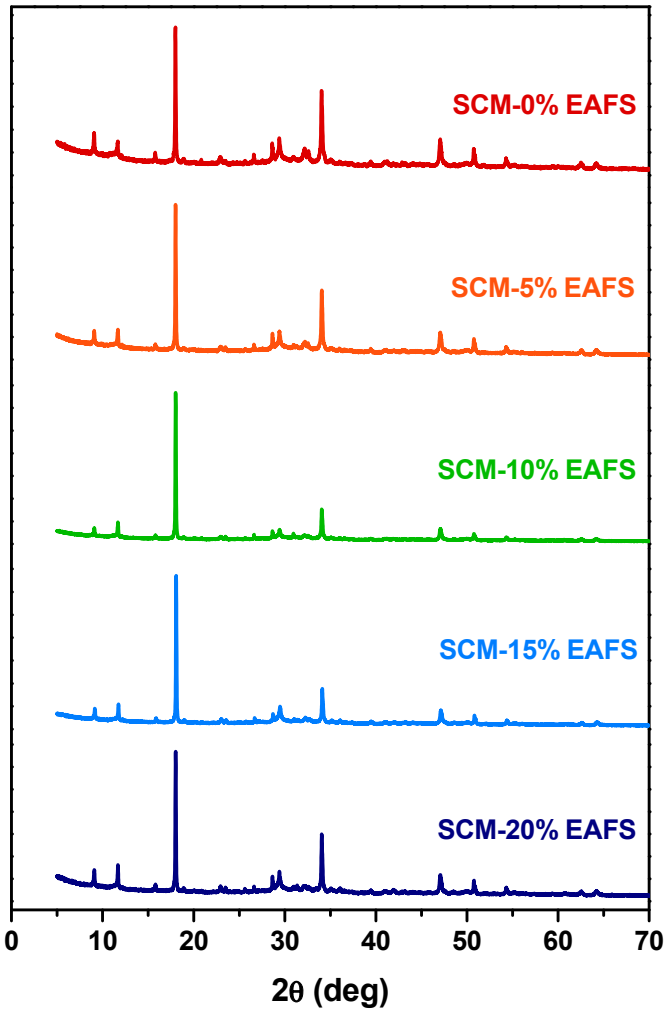


Figure 6. XRD patterns for cement control and cement-EAFS pastes after 28 days.

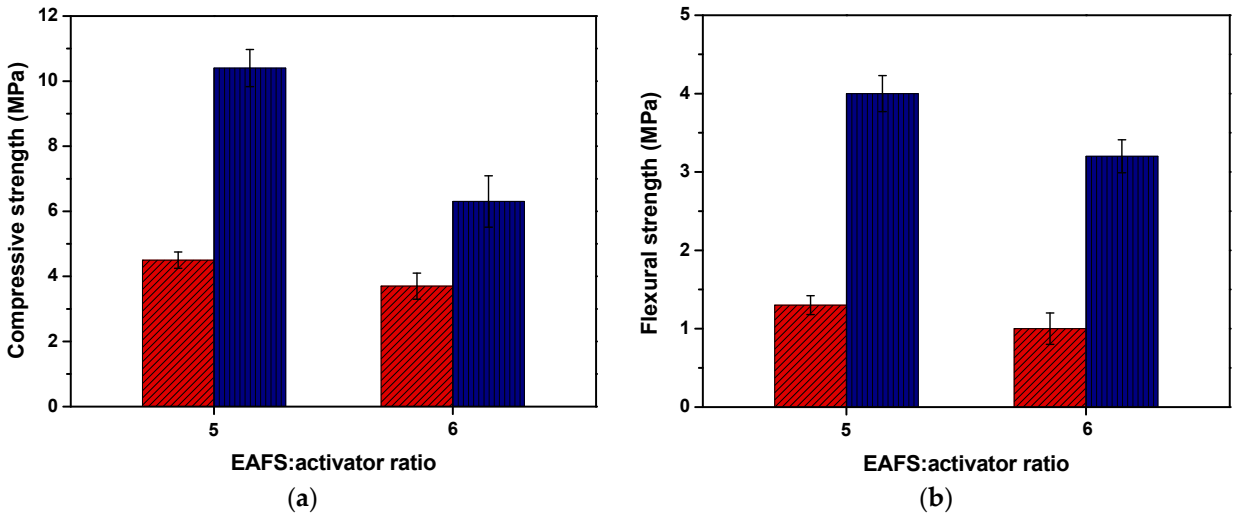


Figure 7. Compressive (n = 6) (**a**) and flexural (n = 3) (**b**) strength (mean values ± standard deviation) for the alkali-activated 100% EAFS composites at 7 days (red) and 28 days (blue).

The compressive strength results for the alkali-activated EAFS composites after 7 and 28 days indicated that increasing the proportion of alkaline activator (from 14.3 wt.% present in AA-6EAFS to 16.7 wt.% in AA-5EAFS) enhances the compressive strength. Furthermore, a significant increase in the compressive strength of the alkali-activated

EAFS composites can be observed from the seventh to the twenty-eighth day of curing. The results for the alkali-activated EAFS composites after 28 days showed a compressive strength of up to 131% higher when compared to the alkali-activated EAFS composites after 7 days.

The development of compressive strength can be explained by the incorporation of EAFS with aluminosilicates and calcium in its composition, which, in the presence of the alkaline activator (sodium silicate), originates the formation of reaction products with binding properties.

However, it is possible to verify that the alkali-activated EAFS composites acquired moderate compressive strength. This fact can be aggravated by the low workability of mixtures containing EAFS. According to the literature [73,74], an increase in steel by-product content typically leads to reduced workability, as finer materials require a greater amount of water content, resulting in a less fluid mixture. Furthermore, it is important to mention that the high-water absorption properties of EAFS can also be a dominant factor in reducing the workability of the mixtures.

Regarding to the flexural strength, the alkali-activated EAFS composites exhibited a similar behaviour to compressive strength results, i.e., a significant increase in the flexural strength (up to 220%) with the increase in the alkaline activator proportion and curing time. The compressive and flexural strength results for the alkali-activated EAFS composites at 7 and 28 days are summarized in Table 7.

Table 7. Compressive (n = 6) and flexural (n = 3) strength (mean ± standard deviation) for the alkali-activated EAFS composites at 7 and 28 days.

Sample Reference	Compressive Strength (MPa)		Flexural Strength (MPa)	
	7 Days	28 Days	7 Days	28 Days
AA (control) [1]	–	–	–	–
AA-5EAFS	4.50 ± 0.25	10.4 ± 0.57	1.30 ± 0.12	4.00 ± 0.23
AA-6EAFS	3.70 ± 0.40	6.30 ± 0.79	1.00 ± 0.20	3.20 ± 0.21

[1] Sample breakdown during the demoulding process.

An attempt to identify the reaction products that may be related to the enhancement of compressive and flexural strength on the alkali-activated EAFS composites using XRD analysis. In addition to the mixtures with the previously analysed proportions, other mixtures with variations in the precursor and alkaline activator ratio were included in this study (3 and 4). The XRD patterns for all the alkali-activated EAFS pastes are presented in Figure 8. According to the results, it was not possible to identify new phases in the diffractograms of the alkali-activated EAFS composites besides those already identified in the EAFS (e.g., wüstite, gehlenite, calcium magnesium silicate, and magnetite), which can be attributed to the fact that the new reacting products responsible for binding the EAFS particles have an amorphous structure [75].

2.2.3. Accelerated Carbonation

The compressive and flexural strength results for the cement control, cement-EAFS, and EAFS carbon accelerated specimens after 7 and 28 days are presented in Figure 9. After 7 days, the compression strength of the cement (control sample) and cement-EAFS carbon accelerated specimens showed comparable values. However, by 28 days, the cement-EAFS specimens exhibited a moderate reduction (16%) in the compressive strength compared to the cement control specimens. On the other hand, the EAFS carbon accelerated specimens presented, as expected, a significantly lower compressive strength. The small increase in the compressive strength with CO_2 curing time can be attributed to the rapid carbonation

reaction occurring in the early days and the denser microstructure that is expected to be formed during the carbonation process, which makes it difficult for CO_2 to penetrate the specimen [76].

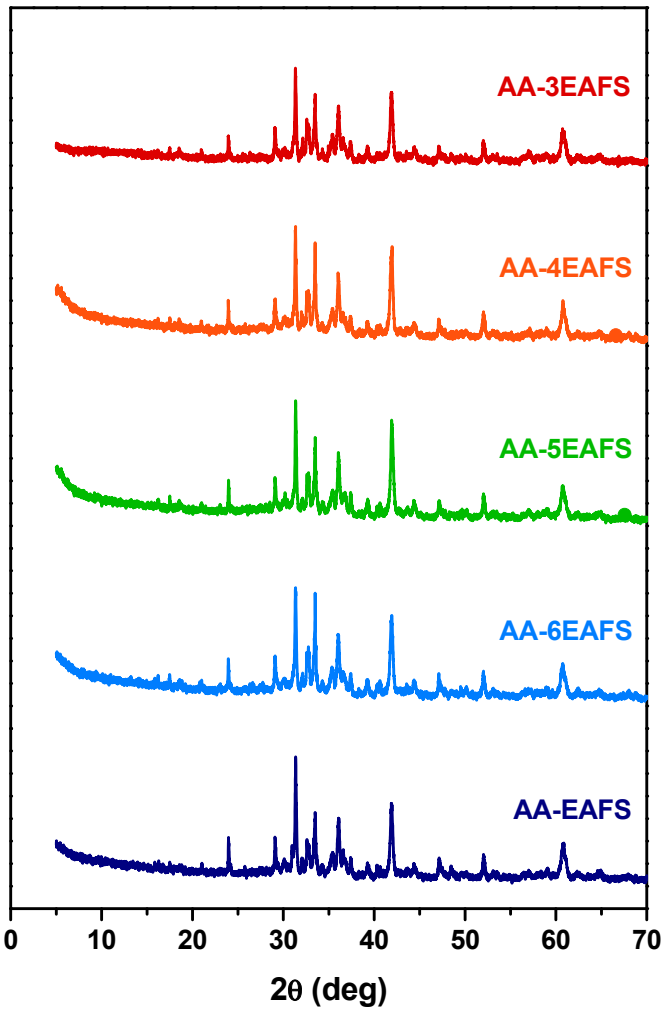


Figure 8. XRD patterns of the EAFS control and alkali-activated EAFS pastes.

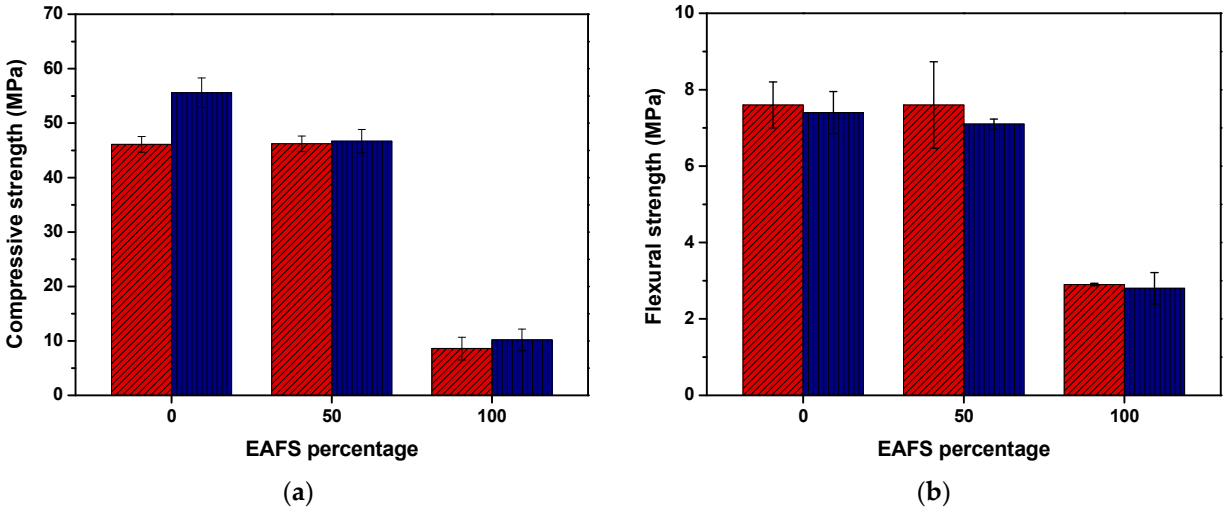


Figure 9. Compressive (n = 6) (**a**) and flexural (n = 3) (**b**) strength (mean values ± standard deviation) for the cement control, cement-EAFS, and EAFS carbon accelerated-based specimens at 7 days (red) and 28 days (blue).

The results obtained for the cement-EAFS carbon accelerated specimens suggest that accelerated carbonation can be an alternative mechanism to enhance the binding properties of this steel co-product, as exceptionally high compressive strength values are maintained even with a 50% replacement of cement by EAFS. Notably, compressive strength levels comparable to those of the cement control specimens that did not undergo the accelerated carbonation process (SCM-0% EAFS) were achieved (see Figure 5). Furthermore, it is possible to observe the positive effect of accelerated carbonation for the cement control, whose compressive strength increase relative to the cement control specimens without the effect of accelerated carbonation (SCM-0% EAFS) was 18.3%. Note that accelerated carbonation made it possible to replace 50% of cement and 50% of sand and still obtain higher compressive strength values (AC-50% EAFS, Table 8), in comparison to the replacement of only 20% of cement without accelerated carbonation (SCM-20% EAFS, Table 6).

Table 8. Compressive (n = 6) and flexural (n = 3) strength (mean ± standard deviation) for the cement control, cement-EAFS, and EAFS specimens at 7 and 28 days, with accelerated carbonation cure.

Sample Reference	Compressive Strength (MPa)		Flexural Strength (MPa)	
	7 Days	28 Days	7 Days	28 Days
AC-0% EAFS (control)	46.1 ± 1.44	55.6 ± 2.71	7.60 ± 0.60	7.40 ± 0.55
AC-50% EAFS	46.2 ± 1.42	46.7 ± 2.13	7.60 ± 1.13	7.10 ± 0.13
AC-100% EAFS	8.60 ± 2.09	10.2 ± 1.98	2.90 ± 0.03	2.80 ± 0.41

Additionally, the compressive strength of specimens with 100% EAFS subjected to accelerated carbonation (AC-100% EAFS, Table 8) is similar to that obtained with alkaline activation of 100% EAFS specimens when using the highest concentration of activator (AA-6EAFS, Table 7).

The mechanism of the microstructure formation for cement-EAFS specimens under CO_2 curing can be explained by the reaction between the Ca-containing, such as C_3S, C_2S, CaO, $Ca(OH)_2$, and $Ca_3Mg(SiO_4)_2$, from the cement and EAFS, with CO_2 to form calcium silicate hydrates (C–S–H) and stable carbonate products [52]. The hydration and carbonation products fill larger voids, effectively densifying the structure, and bind the EAFS or cement gains, which may result in the improvement of the mechanical strength and durability [77]. The main chemical reactions occurring during carbonation are represented by the following equations (Equations (1)–(4)):

$$CaO + H_2O \rightarrow Ca(OH)_2 \quad (1)$$

$$Ca(OH)_2 + CO_2 \rightarrow CaCO_3 + H_2O \quad (2)$$

$$2(2CaO{\cdot}SiO_2) + CO_2 + 3H_2O \rightarrow 3CaO{\cdot}2SiO_2{\cdot}3H_2O + CaCO_3 \quad (3)$$

$$2(3CaO{\cdot}SiO_2) + 3CO_2 + 3H_2O \rightarrow 3CaO{\cdot}2SiO_2{\cdot}3H_2O + 3CaCO_3 \quad (4)$$

After 7 days, the cement-EAFS carbon accelerated specimens revealed similar flexural strength values compared to the cement control carbon accelerated specimens. However, after 28 days, a slight reduction (2.6%) in the flexural strength was observed, which may result from the higher dispersion of the values recorded for these specimens. Similar to the compressive strength results, the EAFS carbon accelerated specimens presented a low compressive strength after 7 and 28 days compared to the other two specimens. The compressive and flexural strength results for the cement control, cement-EAFS, and EAFS carbon accelerated specimens at 7 and 28 days are summarized in Table 8.

To better understand the accelerated carbonation effect on the cement-EAFS specimens, diffractograms were obtained for pastes containing 100% cement and 100% EAFS with and without the action of accelerated carbonation in the curing process. The XRD patterns for these pastes are presented in Figure 10. As expected, the accelerated carbonation process led to significant microstructural changes in the cement pastes, primarily due to the enrichment of the calcite phase (most intense peak near 30°). In Portland cement-based concrete subjected to the action of accelerated carbonation, there is an increase in the volume of solids and molecular weight, which can be explained by the conversion of portlandite into calcite, a process that is responsible for reducing the permeability of this type of concrete [78,79]. In the case of the EAFS paste, it is also possible to see differences in the microstructure of this type of composite after the process of accelerated carbonation. However, these differences are complex and difficult to interpret.

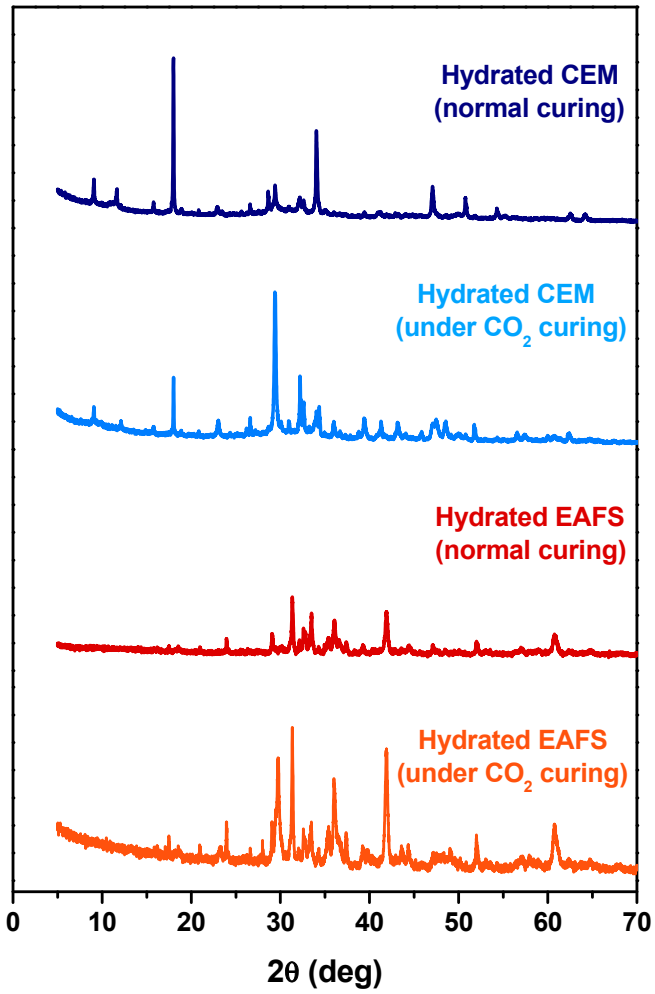


Figure 10. XRD patterns of the hydrated cement and EAFS pastes under normal and accelerated carbonation curing.

In the same way, the identification of the reaction products that may be related to the accelerated carbonation on the cement-EAFS-based pastes by XRD was carried out. In addition to the mixtures with the previously analysed proportions, other mixtures with variations in the cement and EAFS ratio were included in this study. The XRD patterns for all the cement-EAFS carbon accelerated pastes are presented in Figure 11. According to these, it is possible to verify that the characteristic phases of the hydrated cement progressively give rise to new characteristic phases of the reaction products of the EAFS

when subjected to the carbonation process. The identification of the phases found on the patterns are presented in Table 9.

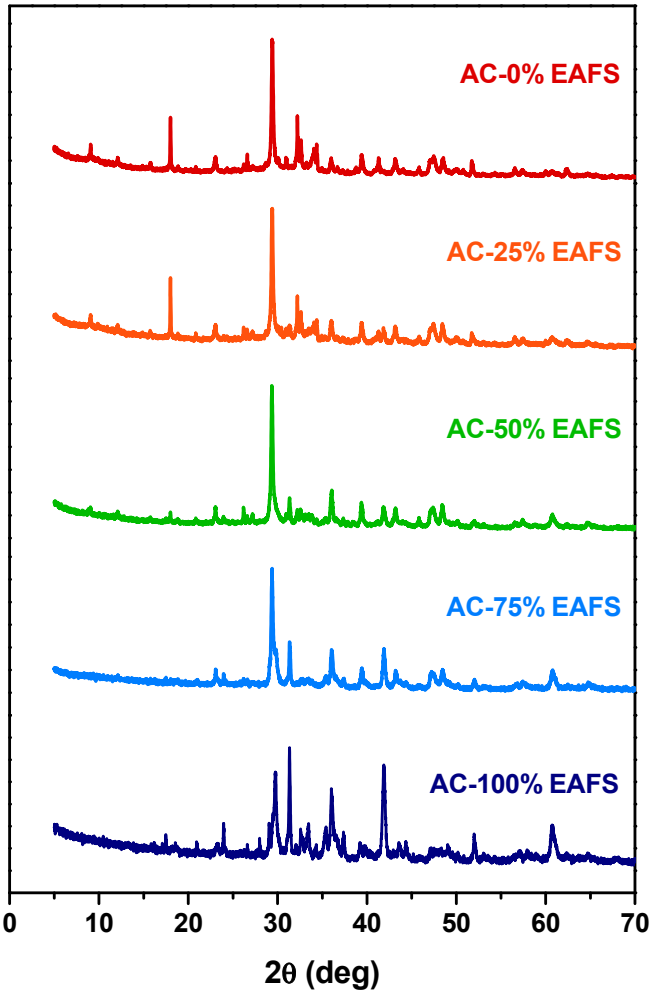


Figure 11. XRD patterns of the cement control, cement-EAFS, and EAFS accelerated carbonation pastes.

Table 9. Identification of the phases found in the XRD patterns of the cement control, cement-EAFS, and EAFS carbon accelerated pastes (the symbol "×" identifies the presence of the compound, while the symbol "–" identifies the absence of the compound).

ICDD	Compound	Structure	AC-0% EAFS (Control)	AC-25% EAFS	AC-50% EAFS	AC-75% EAFS	AC-100% EAFS
01-086-0174	Calcite, syn	$CaCO_3$	×	×	×	×	–
01-086-0402	Hatrurite, syn	Ca_3SiO_5	×	×	×	–	×
00-044-1481	Portlandite, syn	$Ca(OH)_2$	×	×	×	–	–
01-083-2465	Quartz	SiO_2	×	×	×	–	–
01-072-0646	Ettringite	$3CaO{\cdot}Al_2O_3{\cdot}3CaSO_4{\cdot}32H_2O$	×	×	×	–	–
00-030-0226	Brownmillerite, syn	$Ca_2(Al,Fe)_2O_5$	×	×	×	–	–
01-083-0460	Larnite	Ca_2SiO_4	×	×	×	–	–
00-041-1475	Aragonite	$CaCO_3$	–	×	×	–	–

Table 9. *Cont.*

ICDD	Compound	Structure	AC-0% EAFS (Control)	AC-25% EAFS	AC-50% EAFS	AC-75% EAFS	AC-100% EAFS
00-004-0690	Gehlenite	$Ca_2Al_2SiO_7$	–	×	×	×	×
00-006-0615/ 00-003-0968/ 01-075-1550	Wüstite	FeO	–	×	×	×	×
01-075-1610	Magnetite	Fe_3O_4	–	–	×	×	×
01-071-1663	Calcite, magnesian	$Mg_{0.1}Ca_{0.9}CO_3$	–	–	–	×	×
00-034-1350	Calcium, magnesian	$Ca_5MgSi_3O_{12}$	–	–	–	×	×
00-049-0442	Calcium silicate	Ca_3SiO_5	–	–	–	–	×

To synthesise the principal outcomes of this study, Table 10 provides a comparative overview of the advantages and limitations associated with the three EAFS valorisation pathways investigated, namely their use as a supplementary cementitious material (SCM), in alkali-activated systems (AA), and under accelerated carbonation (AC) conditions.

Table 10. Key findings and comparative aspects of the three valorisation pathways concerning the advantages and disadvantages of adding EAFS.

Valorisation Pathway	Advantages	Disadvantages
Supplementary Cementitious Materials (SCM)	• Significant increase in compressive strength at 10% EAFS replacement (51.2 MPa; +8.9% relative to the reference); • Compressive strength comparable to reference mix maintained up to 15% replacement (45.8–47.0 MPa); • Highest absolute compressive strength among all valorisation routes; • Partial reduction of clinker content, contributing to lower CO_2 emissions; • Compatibility with conventional cement production and curing practices.	• Performance highly dependent on replacement level; • Narrow optimal replacement window; • Limited substitution rate compared to conventional SCMs; • Fine grinding required to achieve reactivity, increasing energy demand.

Table 10. *Cont.*

Valorisation Pathway	Advantages	Disadvantages
Alkali Activation (AA)	• High incorporation rates of EAFS as a primary raw material; • Potential clinker-free binder system; • Simultaneous use of fine and coarse EAFS fractions, reducing pre-treatment requirements.	• Very low compressive strength (6.3–10.4 MPa); • Severe strength reductions compared to the reference cement specimens (−77.9% to −86.6%); • Mechanical performance highly dependent on activator type and dosage; • Limited understanding of long-term durability; • Limited structural applicability under tested conditions.
Accelerated Carbonation (AC)	• Enables very high incorporation of EAFS as the main binder component, as well as coarse fractions; • High compressive strength maintained at 50% EAFS incorporation (46.7 MPa; 0.6% relative to the reference cement specimens under normal conditions); • Demonstrates effectiveness of carbonation as a strength-enhancing mechanism; • Potential for CO_2 sequestration via mineral carbonation.	• Sharp loss of strength at 100% EAFS incorporation (10.2 MPa; −78.3%); • Strong dependence on EAFS content and carbonation conditions; • Narrow compositional robustness; • Process complexity and need for controlled CO_2 curing conditions; • Energy and infrastructure requirements for accelerated carbonation; • Limited data on long-term durability and scalability.

3. Materials and Methods

3.1. Materials

The electric arc furnace slag in fine fraction (≤2 mm) was sourced from a metallurgy company, Siderurgia Nacional (Maia, Portugal). The material in its original state and ground with a planetary ball mill (PM100, Retsch, Haan, Germany) was used as an aggregate and a reaction precursor, respectively. A Portland cement (OPC) type-II/A-L 42.5 R, manufactured by Secil Group (Maceira-Liz, Portugal) and certified according to the standard EN 197-1 [80], was selected for the preparation of cement and cement-EAFS test specimens. The CEM-II/A-L 42.5 R was composed of 80–94% Portland clinker without special specifications, 6–20% calcium carbonate fines, and 0–5% gypsum by weight, with a specific gravity of 3.1 Mg/m^3. A siliceous fine aggregate of washed sand (S0/4), provided by Sabril-Sociedade de Areias e Britas, Lda. (Pombal, Portugal), was used as mineral aggregates. A commercial concentrated sodium silicate solution (Na_2SiO_3), provided by Marcande-Engenharia Química e Civil, Lda. (Guimarães, Portugal), was used as alkali activator.

3.2. Test Specimens

In this study, several mixes were prepared containing different amounts of EAFS in its original state and/or ground, depending on the alternative waste-to-value approach

under assessment. Control specimens without EAFS were also prepared for the purpose of comparing the results. For each case, three prismatic test specimens with dimensions of 160 mm × 40 mm × 40 mm were prepared. Detailed information regarding the mixing, preparation, and curing procedures is given in the following sections.

3.2.1. Cement-EAFS Specimens

To investigate the potential of the EAFS (ground) as a partial substitute for cement and its influence on the properties of cement-EAFS composites, different EAFS for Portland cement replacement ratios of 0, 5, 10, 15, and 20% were evaluated. Detailed information on the mix proportions of CEM-II 42.5, EAFS, sand (S0/4), and water is presented in Table 11. The cement-EAFS mortars were prepared in a laboratory mixer, transferred to steel moulds, and compacted using a jolting apparatus. After an initial curing period of 24 h in polyethylene bags, the specimens were demoulded and stored in a temperature- and humidity-controlled room (T = 20 ± 2 °C, RH ≥ 95%) until the testing days.

Table 11. Mix proportions of the cement control and cement-EAFS specimens.

Sample Reference	Quantities per Batch (g) for Three 256-cm^3 Specimens			
	CEM-II 42.5	EAFS (Ground)	S0/4	Water
SCM-0% EAFS (control)	450.0	0.0	1350	225
SCM-5% EAFS	427.5	22.5	1350	225
SCM-10% EAFS	405.0	45.0	1350	225
SCM-15% EAFS	382.5	67.5	1350	225
SCM-20% EAFS	360.0	90.0	1350	225

3.2.2. Alkali-Activated EAFS Specimens

To investigate the potential of alkali-activated EAFS, test specimens were produced using EAFS in its original and ground states. For that, the amounts of ground and granulated slag were kept in the same proportion of cement and sand used in the previous study, while the proportions of alkali-activator and water were varied. Detailed information on the mix proportions of the alkali-activated specimens is presented in Table 12. The indices "5" and "6" in AA-5EAFS and AA-6EAFS sample references refer to the ratio between the total EAFS weight and activator weight. The alkali-activated mortars were prepared in a laboratory mixer, transferred to marine plywood moulds, and mechanically compacted, applying a load of 16 tonnes with a manual press. After an initial curing period of 24 h at 60 °C, the specimens were demoulded and stored in a temperature- and humidity-controlled room (T = 20 ± 2 °C, RH ≥ 95%) until the testing days.

Table 12. Mix proportions of the EAFS control and alkali-activated EAFS specimens.

Sample Reference	Quantities per Batch (g) for Three 256-cm^3 Specimens			
	EAFS (Ground)	EAFS (Original)	Activator	Water
AA-EAFS (control)	450	1350	0	360
AA-5EAFS	450	1350	360	0
AA-6EAFS	450	1350	300	60

3.2.3. Carbon Accelerated Cement-EAFS Specimens

To investigate the potential of EAFS and the effect of accelerated carbonation on the properties of cement-EAFS and EAFS materials, test specimens with and without EAFS in its original and ground states were prepared. Detailed information on the mix proportion of the specimens subjected to accelerated carbonation conditions is presented in Table 13.

Based on the particle size characteristics and reactivity potential, the authors chose to replace cement and sand with the ground and non-ground EAFS, respectively. This was expected to allow a higher percentage of the original raw materials to be replaced, without compromising the mechanical properties of the hardened specimens. Additionally, a cement- and sand-free composition was tested to compare its results with those obtained from alkali activation intended for non-structural applications.

Table 13. Mix proportions of the cement control, cement-EAFS, and EAFS specimens subjected to accelerated carbonation.

Sample Reference	Quantities per Batch (g) for Three 256-cm^3 Specimens				
	CEM-II 42.5	**EAFS (Ground)**	**EAFS (Original)**	**S0/4**	**Water**
AC-0% EAFS (control)	450	0	0	1350	225
AC-50% EAFS	225	225	675	675	225
AC-100% EAFS	0	450	1350	0	225

The carbon accelerated-based specimens were prepared in a laboratory mixer, transferred to steel moulds, and compacted using a jolting apparatus. After an initial curing period of 7 days in a temperature- and humidity-controlled chamber (T = 60 °C, RH = 90%) with atmosphere partially replaced by CO_2 (70%), part of the specimens were demoulded and submitted to tests, while the other part was stored in a temperature- and humidity-controlled room (T = 20 ± 2 °C, RH ≥ 95%) until 28 days before testing.

3.3. Methods

3.3.1. Particle Dimension

The maximum dimension and particle size analyses were carried out in accordance with the standard EN 933-1 by the sieving method [81] and by laser diffraction (Mastersizer 2000, Malvern Panalytical, Malvern, UK). The loose bulk density and percentage of voids were determined in accordance with the standard EN 1097-3 [82]. The particle density and water absorption were evaluated according to standard EN 1097-6 [83].

3.3.2. X-Ray Fluorescence

Representative portions of the raw materials were collected, ground in a planetary ball mill (PM 100, Retsch), and passed through a 100 µm mesh sieve. Pressed pellets were obtained by compressing at 20 tonnes for 2 min the powdered raw materials with a binder (Licowax®, CEREOX, Bedburg-Hau, Germany) using a manual press (ECH3000/600/4C, Microtest, Tocha, Portugal). The chemical composition was analysed using the pressed pellets by wavelength dispersive X-ray fluorescence (WD-XRF) spectrometry (Supermini 200 sequential spectrometer with Pd X-ray tube and X-ray generator operating under 50 kV and 4.00 mA, Rigaku, Neu-Isenburg, Germany). Elemental mass percentages were calculated (Rigaku ZSX Primus). Loss of ignition (LOI) was measured by heating 5.0 g of oven-dried samples to 975 °C in porcelain crucibles for 1 h.

3.3.3. X-Ray Diffraction

The crystalline mineralogical phases were evaluated by powder X-ray diffraction (PXRD) analysis using a Rigaku Smartlab® diffractometer with a 2.2 kW Cu sealed-tube X-ray source (λ = 0.15406 nm). The patterns were collected at room temperature over a 2θ range of 5–70°, with 0.01° steps, 1°/min, and 10 rpm, using a 2θ-θ coupled mode Bragg–Brentano geometry, with the diffractometer operating at 40 kV and 50 mA. The PXRD patterns were analysed by Rietveld method using SmartLab Studio II [84]. For clarity,

complete peak identification and phase attribution for all diffractograms are provided in the Supplementary Materials.

3.3.4. Release of Dangerous Substances

Aqueous extracts of the EAFS were obtained following the standard EN 12457-2 [85], using a single-stage batch leaching test with a 24 h extraction period and a liquid-to-solid ratio (L/S) of 10 L/kg of dry material. The procedure involved mixing the sample with an appropriate amount of deionized water in a polypropylene container, followed by continuous agitation at 10 rpm on a rotary shaker (Rotax 6.8 overhead mixer, VELP Scientifica, Lisboa, Portugal). This method, designed to evaluate the leachable chemical components from waste materials, operates under the assumption that equilibrium or near-equilibrium conditions are reached between the liquid and solid phases during testing. After the extraction period, the solid fraction was separated by filtration (0.45 μm pore filter). Additionally, for the total content of organic parameters, organic extracts were produced directly from the EAFS. The aqueous and organic extracts were then analysed by inductively coupled plasma optical emission spectrometry (Optima 8000, Perkin Elmer, Waltham, USA), gas chromatography associated with mass spectrometry (SCION 456-GC, EVOQ TQ MS, Bruker, Paço de Arcos, Portugal), liquid chromatography (Flexar uHPLC, Perkin Elmer, Waltham, USA), combustion-infrared (multi N/C 3100, Analytik-Jena, Jena, Germany), and other classic chemical methods.

3.3.5. Pozzolanicity

The pozzolanic activity of EAFS was determined by Frattini test with adaptations of the procedure specified in the standard EN 196-5 [64]. In total, 20 g of test samples were prepared, consisting of 80% CEM-II 42.5 and 20% EAFS and mixed with 100 mL of distilled water. In the same way, control samples containing 100% CEM-II 42.5, 80% cement CEM-II 42.5, and 20% metakaolin (MK), a known pozzolan, were prepared. Following preparation, the samples were stored in a sealed plastic bottle inside an oven at 40 °C for periods of 8 and 15 days. At the end of each period, the samples were vacuum-filtered using a 2.7 μm nominal pore size filter paper (Whatman No. 542) and allowed to cool to ambient temperature in sealed Buchner funnels. The filtrate was then analysed to determine $[OH^-]$ by titration against diluted HCl with methyl orange indicator. The $[Ca^{2+}]$ was assessed by adjusting the pH to 12.5, followed by complexometric titration with 0.03 mol/L EDTA solution in the presence of Patton–Reeders indicator.

3.3.6. Isothermal Calorimetry

The influence of EAFS on the hydration heat of cementitious pastes was evaluated by isothermal calorimetry in accordance with the standard ASTM C1702 [86]. The evolution of hydration heat rate and cumulative heat of different cementitious systems was monitored at 23 ± 1 °C using a four-channel isothermal calorimeter (I-Cal 4000 HPC, Calmetrix, Porto, Portugal). Before the test, the calorimeter units were calibrated in accordance with the manufacturer's specifications.

To ensure the cement content and a proper measurement temperature, the accurate amount of liquid was first measured and left for at least 2 h inside the calorimeter cell to stabilise at 23 °C. Meanwhile, cement and EAFS were weighed, and the cement pastes were mixed directly inside the sample vials that were later placed inside the calorimeter cells. All pastes had a fixed precursor (cement and EAFS) weight of 40 g and water weight of 20 g; pastes with EAFS incorporated had the cement mass deducted from the added EAFS. The experimental design is detailed in Table 14. The paste components were manually mixed for 30 s using a plastic spoon, which remained inside the sample cup to prevent material loss. The isothermal calorimeter measures the heat flow by means of a heat flow sensor,

which is under the sample cup and in contact with a heat sink. To determine the hydration heat of each sample, the measured thermal powers were integrated from the beginning to 48 h. Data acquisition occurred at 1 min intervals. The results obtained were normalised by the amount of cement (g cement), ensuring that the changes in the heat-release profiles of the mixes are solely a function of the amount of slag.

Table 14. Cement control and cement-EAFS pastes used in the hydration heat evaluation.

Sample Reference	CEM-II 42.5 (g)	EAFS (Ground) (g)	Water (g)
CEM-II 42.5 (control)	40	0	20
CEM-II 42.5 + 5% EAFS	38	2	20
CEM-II 42.5 + 10% EAFS	36	4	20
CEM-II 42.5 + 15% EAFS	34	6	20
CEM-II 42.5 + 20% EAFS	32	8	20

3.3.7. Mechanical Characterisation

The mechanical performance of the cement control, cement-EAFS, and EAFS specimens was evaluated through flexural and compressive strength tests at 7 and 28 days. Both tests were conducted using a universal testing machine (model 59R5884, with a load cell of 10 kN, Instron). The load was applied without shock at a uniform rate of 10 N/s and 50 N/s in the flexural and compressive strength tests, respectively. For each mix, three prismatic specimens (160 mm × 40 mm × 40 mm) were prepared, allowing for three flexural strength tests (n = 3) and six compressive strength tests (n = 6). The span between the support rollers for the flexural strength test was 100 mm. The compressive strength was determined from the two parts provided by the flexural strength test, according to EN 12390-3 [87].

4. Conclusions

This work was aimed to investigate different approaches to enhance the reactive potential of an electric arc furnace slag (EAFS) to produce more ecological binders. First, EAFS was characterised in terms of chemical and mineralogical composition, release of dangerous substances, pozzolanic activity, and influence on cement hydration heat. Subsequently, the reactive potential of EAFS was investigated using it as a supplementary cementitious material, or as a raw material to be alkali-activated, and submitted to accelerated carbonation process. Compressive and flexural strengths of hardened materials produced were tested at different curing ages. Based on the experimental results, the following conclusions can be drawn:

- As supplementary cementitious material, the EAFS produced an increase in the compressive strength of hardened specimens at a cement replacement level of 10% (+4.2 MPa), while reduced losses in compressive strength were observed at replacement levels of 5%, 15%, and 20% (−5.8, −1.2, and −6.6 MPa, respectively). The calorimetric and XRD results further suggest that EAFS can act as a reagent source for limiting components of the cement hydration reactions and that an optimal ratio, from the stoichiometric point of view, between the amount of cement and EAFS seems to occur for cement replacement values close to 10%. Nevertheless, EAFS may be responsible for disruptive effects in the cement matrix due to nonreactive phases or an excess of unreacted particles.
- Using the alkali-activation route, moderate compressive strengths were developed. This can be explained by the presence of aluminosilicates and calcium in the composition of EAFS, which are known to form reaction products with binding properties in the presence of suitable alkaline activators. However, it was not possible to characterise the newly formed reaction products by XRD due to their likely amorphous

structure. The results also show that higher amounts of alkaline activator led to higher compressive strengths (from 6.3 MPa at 14.3 wt.% activator to 10.4 MPa at 16.7 wt.% activator), suggesting that optimal stoichiometric conditions may be further studied to improve the mechanical properties of the hardened material obtained by this valorisation pathway.

- As expected, the accelerated carbonation process revealed an increase in the compressive strength of the cement control (from 47.0 MPa under normal curing to 55.6 MPa after accelerated carbonation at 28 days curing). Additionally, a very high compressive strength was maintained even with a replacement of 50% of cement and sand by ground EAFS and granulated EAFS, respectively (46.7 MPa after carbonation curing), suggesting that this process can be an alternative reaction pathway to explore the binding properties of EAFS. The XRD results also show that, with increasing EAFS content (from 0% to 50% replacement), most characteristic phases of hydrated cement progressively give rise to new phases associated with the reaction products of the cement–EAFS and EAFS–EAFS systems.

Based on the results described, the authors believe that the reactivity of EAFS can be improved, allowing their use in added-value applications beyond the current basic replacement of virgin coarse and fine aggregates in concrete. This comparative study provided insights into the versatility of EAFS as a secondary raw material and supports its potential integration into diverse low-clinker or alternative binder technologies. However, further studies should be conducted to deepen the optimal conditions and assess practical implications of manufacturing and durability, including economic costs and environment performance in terms of life cycle analysis.

Supplementary Materials: The following supporting information can be downloaded at: https://www.mdpi.com/article/10.3390/recycling11020025/s1, Figure S1: XRD powder pattern of EAFS (Figure 2—top, in the paper) with full identification of mineralogical phases; Figure S2: XRD powder pattern of CEM-II 42.5 (Figure 2, bottom, in the paper) with full identification of mineralogical phases; Figure S3: XRD powder pattern of SCM-0% paste after 28 days (Figure 6, in the paper) with full identification of mineralogical phases; Figure S4: XR patterns for cement control and cement-EAFS pastes after 28 days (Figure 6 in the paper); Figure S5: XRD pattern of the AA-EAFS paste (Figure 8 in the paper) with full identification of mineralogical phases; Figure S6: XRD pattern of the AC-0% EAFS paste (Figure 11 in the paper) with full identification of mineralogical phases; Figure S7: XRD pattern of the AC-25% EAFS paste (Figure 11 in the paper) with full identification of mineralogical phases; Figure S8: XRD pattern of the AC-50% EAFS paste (Figure 11 in the paper) with full identification of mineralogical phases; Figure S9: XRD pattern of the AC-75% EAFS paste (Figure 11 in the paper) with full identification of mineralogical phases; Figure S10: XRD pattern of the AC-100% EAFS paste (Figure 11 in the paper) with full identification of mineralogical phases.

Author Contributions: Conceptualization, P.H., J.A. (Julieta António) and J.A. (João Almeida); validation, B.M.; investigation, B.M. and D.S.; writing—original draft preparation, B.M., D.S. and J.A. (João Almeida); writing—review and editing, J.A. (Julieta António); supervision, J.A. (Julieta António) and J.A. (João Almeida); project administration, J.A. (João Almeida); funding acquisition, P.H. All authors have read and agreed to the published version of the manuscript.

Funding: This research was funded by the Fundação para a Ciência e a Tecnologia, I.P. (FCT, https://ror.org/00snfqn58, accessed on 22 January 2026) under the project InnoCreteTech, grant EXPL/ECI-EGC/1585/2021, and under Grant UID/6438/2025 (https://doi.org/10.54499/UID/06438/2025, accessed on 22 January 2026) of the research unit CERIS. The authors acknowledge the Portuguese Pluriannual Base Funding for Technology and Innovation Centres (Call No 03/C05-i02/2022) as part of the Mission Interface supported by the Recovery and Resilience Plan (RRP) and Next Generation EU mechanisms.

Data Availability Statement: The data presented in this study are sufficient for the purposes of this investigation; however, they are available for further analysis upon request from the corresponding author.

Acknowledgments: The authors are grateful to Siderurgia Nacional, Secil Group, and Sabril-Sociedade de Areias e Britas, Lda., which kindly supplied the raw materials used in this study: EAFS, cement, and mineral aggregates, respectively.

Conflicts of Interest: The authors declare no conflicts of interest.

References

1. Singh, R.L.; Singh, P.K. Global Environmental Problems. In *Principles and Applications of Environmental Biotechnology for a Sustainable Future*; Singh, R.L., Ed.; Springer: Singapore, 2017; pp. 13–41.
2. Mathur, V.S.; Farouq, M.M.; Labaran, Y.H. The Carbon Footprint of Construction Industry: A Review of Direct and Indirect Emission. *J. Sustain. Constr. Mater. Technol.* **2021**, *6*, 101–115. [CrossRef]
3. Labaran, Y.H.; Mathur, V.S.; Muhammad, S.U.; Musa, A.A. Carbon Footprint Management: A Review of Construction Industry. *Clean. Eng. Technol.* **2022**, *9*, 100531. [CrossRef]
4. Andrew, R.M. Global CO2 Emissions from Cement Production, 1928–2018. *Earth Syst. Sci. Data* **2019**, *11*, 1675–1710. [CrossRef]
5. Cormos, C.C. Decarbonization Options for Cement Production Process: A Techno-Economic and Environmental Evaluation. *Fuel* **2022**, *320*, 123907. [CrossRef]
6. Council of the European Union. Directive 2008/98/EC of the European Parliament and of the Council of 19 November 2008 on Waste and Repealing Certain Directives. *Off. J. Eur. Union* **2008**, *312*, 3–30.
7. Council of the European Union. Directive (EU) 2018/851 of the European Parliament and of the Council of 30 May 2018 Amending Directive 2008/98/EC on Waste (Text with EEA Relevance). *Off. J. Eur. Union* **2018**, *150*, 109–140.
8. European Commission. Communication from the Commission to the European Parliament, the Council, the European Economic and Social Committee and the Committee of the Regions: European Climate Pact, COM(2020) 788 Final. 9 December 2020. Available online: https://eur-lex.europa.eu/legal-content/EN/ALL/?uri=COM:2020:788:FIN (accessed on 22 January 2026).
9. Scrivener, K.L.; John, V.M.; Gartner, E.M. Eco-Efficient Cements: Potential Economically Viable Solutions for a Low-CO2 Cement-Based Materials Industry. *Cem. Concr. Res.* **2018**, *114*, 2–26. [CrossRef]
10. World Steel Association. *Steel Industry Co-Products*; World Steel Association: Brussels, Belgium, 2020.
11. Branca, T.A.; Colla, V.; Algermissen, D.; Granbom, H.; Martini, U.; Morillon, A.; Pietruck, R.; Rosendahl, S. Reuse and Recycling of By-Products in the Steel Sector: Recent Achievements Paving the Way to Circular Economy and Industrial Symbiosis in Europe. *Metals* **2020**, *10*, 345. [CrossRef]
12. Parron-Rubio, M.E.; Perez-Garcia, F.; Gonzalez-Herrera, A.; Oliveira, M.J.; Rubio-Cintas, M.D. Slag Substitution as a Cementing Material in Concrete: Mechanical, Physical and Environmental Properties. *Materials* **2019**, *12*, 2845. [CrossRef] [PubMed]
13. Tsakiridis, P.E.; Papadimitriou, G.D.; Tsivilis, S.; Koroneos, C. Utilization of Steel Slag for Portland Cement Clinker Production. *J. Hazard. Mater.* **2008**, *152*, 805–811. [CrossRef]
14. Ryu, G.U.; Kim, H.J.; Yu, H.J.; Pyo, S. Utilization of Steelmaking Slag in Cement Clinker Production: A Review. *J. CO2 Util.* **2024**, *84*, 102842. [CrossRef]
15. Dondi, G.; Mazzotta, F.; Lantieri, C.; Cuppi, F.; Vignali, V.; Sangiovanni, C. Use of Steel Slag as an Alternative to Aggregate and Filler in Road Pavements. *Materials* **2021**, *14*, 345. [CrossRef]
16. Asmatulaev, B.A.; Asmatulaev, R.B.; Abdrasulova, A.S.; Levintov, B.L.; Vitushchenko, M.F.; Stolyarskiiv, O.A. Using Blast-Furnace Slag in Road Construction. *Steel Transl.* **2007**, *37*, 722–725. [CrossRef]
17. Sukmak, P.; Sukmak, G.; De Silva, P.; Horpibulsuk, S.; Kassawat, S.; Suddeepong, A. The Potential of Industrial Waste: Electric Arc Furnace Slag (EAF) as Recycled Road Construction Materials. *Constr. Build. Mater.* **2023**, *368*, 130393. [CrossRef]
18. Yang, J.; Ma, R.; Dong, B.; Ma, H.; Wang, Y.; Gao, M.; Sun, Y.; Jin, Y. Research Progress and Hotspots of Steel Slag Application in Road Construction: A Bibliometric Perspective. *Infrastructures* **2025**, *10*, 54. [CrossRef]
19. López-Díaz, A.; Ochoa-Díaz, R.; Grimaldo-León, G.E. Use of BOF Slag and Blast Furnace Dust in Asphalt Concrete: An Alternative for the Construction of Pavements. *DYNA* **2018**, *85*, 24–30. [CrossRef]
20. Pasetto, M.; Baldo, N. Experimental Evaluation of High Performance Base Course and Road Base Asphalt Concrete with Electric Arc Furnace Steel Slags. *J. Hazard. Mater.* **2010**, *181*, 938–948. [CrossRef]
21. Yu, L.; Lei, B.; Lv, Z.; Zhao, H.; Jiang, W.; Wang, E. Microstructural Evolution and Damage Modeling of Steel Slag Asphalt Concrete under Combined Salt Freeze-Thaw Cycling and Cyclic Preloading Conditions. *Int. J. Fatigue* **2026**, *204*, 109338. [CrossRef]
22. Branca, T.A.; Pistocchi, C.; Colla, V.; Ragaglini, G.; Amato, A.; Tozzini, C.; Mudersbach, D.; Morillon, A.; Rex, M.; Romaniello, L. Investigation of (BOF) Converter Slag Use for Agriculture in Europe. *Metall. Res. Technol.* **2014**, *111*, 155–167. [CrossRef]
23. Kimio, I. Steelmaking Slag for Fertilizer Usage. *Nippon Steel Sumitomo Met. Tech. Rep.* **2015**, *109*, 130–136.

24. Yi, H.; Xu, G.; Cheng, H.; Wang, J.; Wan, Y.; Chen, H. An Overview of Utilization of Steel Slag. *Procedia Environ. Sci.* **2012**, *16*, 791–801. [CrossRef]
25. Goswami, V.; Deepika, S.; Sharma, P.; Kothamasi, D. Recycling Steel Slag as Fertiliser Proxy in Agriculture Is Good Circular Economy but Disrupts Plant Microbial Symbioses in the Soil. *Sci. Total Environ.* **2024**, *954*, 176750. [CrossRef]
26. O'Connor, J.; Nguyen, T.B.T.; Honeyands, T.; Monaghan, B.; O'Dea, D.; Rinklebe, J.; Vinu, A.; Hoang, S.A.; Singh, G.; Kirkham, M.B.; et al. Production, Characterisation, Utilisation, and Beneficial Soil Application of Steel Slag: A Review. *J. Hazard. Mater.* **2021**, *419*, 126478. [CrossRef]
27. Ghisman, V.; Muresan, A.C.; Buruiana, D.L.; Axente, E.R. Waste Slag Benefits for Correction of Soil Acidity. *Sci. Rep.* **2022**, *12*, 16042. [CrossRef]
28. Lin, X.; Peng, Z.; Yan, J.; Li, Z.; Hwang, J.Y.; Zhang, Y.; Li, G.; Jiang, T. Pyrometallurgical Recycling of Electric Arc Furnace Dust. *J. Clean. Prod.* **2017**, *149*, 1079–1100. [CrossRef]
29. Xue, Y.; Hao, X.; Zhang, N. Recovery of Zinc and Iron from Steel Mill Dust—An Overview of Available Technologies. *Materials* **2022**, *15*, 4127. [CrossRef]
30. García, S.G.; Montequín, V.R.; Fernández, R.L.; Fernández, F.O. Evaluation of the Synergies in Cogeneration with Steel Waste Gases Based on Life Cycle Assessment: A Combined Coke Oven and Steelmaking Gas Case Study. *J. Clean. Prod.* **2019**, *217*, 576–583. [CrossRef]
31. Zhang, S.; Ghouleh, Z.; Mucci, A.; Bahn, O.; Provençal, R.; Shao, Y. Production of Cleaner High-Strength Cementing Material Using Steel Slag under Elevated-Temperature Carbonation. *J. Clean. Prod.* **2022**, *342*, 130948. [CrossRef]
32. Zhang, L.; Cui, J.; Chen, Z.; Jing, X.; Liu, Y.; He, B.; Cang, D. Recycling of Carbonated Steel Slag in Building Materials: Recycling Pathways and Recent Advances. *J. Build. Eng.* **2025**, *104*, 112285. [CrossRef]
33. Yang, K.; Aslani, F.; Dyskin, A.; Pasternak, E. Carbon-Negative Slag-Based Binders: A Review of Steel Slags. *J. Build. Eng.* **2026**, *118*, 115068. [CrossRef]
34. Zhang, N.; Deng, G.; Liao, W.; Ma, H.; Hu, C. Aqueous Carbonation of Steel Slags: A Comparative Study on Mechanisms. *Cem. Concr. Compos.* **2025**, *155*, 105838. [CrossRef]
35. Mohammed, T.O.; Ul Haq, A.; Harun, M.Z.B.; Fanijo, E.O. Recent Advances in Fly Ash- and Slag-Based Geopolymer Cements. *Sustainability* **2025**, *17*, 11167. [CrossRef]
36. Amer, I.; Abdelkhalik, A.; Mayhoub, O.A.; Kohail, M. Development of Sustainable Slag-Based Geopolymer Concrete Using Different Types of Chemical Admixtures. *Int. J. Concr. Struct. Mater.* **2024**, *18*, 27. [CrossRef]
37. Khair, S.; Rahman, S.A.; Shaikh, F.U.A.; Sarker, P.K. Evaluating Lithium Slag for Geopolymer Concrete: A Review of Its Properties and Sustainable Construction Applications. *Case Stud. Constr. Mater.* **2024**, *20*, e02822. [CrossRef]
38. Hashem, F.S.; Salam, A.T.A.; Monir, D. Mechanical Properties and Durability of Slag Granite Geopolymer Cement Incorporated Zirconium Aluminum Layered Double Hydroxide. *Sci. Rep.* **2025**, *15*, 17824. [CrossRef]
39. Gökçe, H.S. Durability of Slag-Based Alkali-Activated Materials: A Critical Review. *J. Aust. Ceram. Soc.* **2024**, *60*, 885–903. [CrossRef]
40. Brand, A.S.; Fanijo, E.O. A Review of the Influence of Steel Furnace Slag Type on the Properties of Cementitious Composites. *Appl. Sci.* **2020**, *10*, 8210. [CrossRef]
41. Li, Y.-F.; Lin, H.-S.; Syu, J.-Y.; Lee, W.-H.; Huang, C.-H.; Tsai, Y.-K.; Shvarzman, A. Investigating the Static and Dynamic Mechanical Properties of Fiber-Reinforced Concrete Incorporating Recycled Carbon Fiber and Modified Basic Oxygen Furnace Slag Aggregate. *Recycling* **2025**, *10*, 206. [CrossRef]
42. Xue, J.C.; Wang, W.C.; Wu, C.H.; Hong, T.J.; Chen, T.H.; Huang, C.Y. Deterioration Analysis and Expansion Behavior Prediction of Electric Arc Furnace Slag as Fine Aggregate in Mortar. *J. Build. Eng.* **2024**, *85*, 108717. [CrossRef]
43. Rojas, N.; Bustamante, M.; Muñoz, P.; Godoy, K.; Letelier, V. Study of Properties and Behavior of Concrete Containing EAF Slag as Coarse Aggregate. *Dev. Built Environ.* **2023**, *14*, 100137. [CrossRef]
44. Lu, Q.; Hua, S.; Yue, H. Effect of Spherical Electric Arc Slag on Solid Waste-Based 3D-Printed Concrete. *Appl. Sci.* **2025**, *15*, 11933. [CrossRef]
45. Mohammed, A.J.; Hassan, M.S.; Al-Quraishi, H.; Sameer, H. Strength, Thermal and Environmental Analysis of Ultrahigh-performance Slag Concrete: Modelling and Optimization Approach. *Eur. J. Environ. Civ. Eng.* **2025**, *29*, 1848–1870. [CrossRef]
46. Khan, M.I.; Abbas, Y.M.; Abellan-Garcia, J.; Castro-Cabeza, A. Eco-Efficient Ultra-High-Performance Concrete Formulation Utilizing Electric Arc Furnace Slag and Recycled Glass Powder–Advanced Analytics and Lifecycle Perspectives. *J. Mater. Res. Technol.* **2024**, *32*, 362–377. [CrossRef]
47. Yue, H.; Wang, X.; Hua, S.; Cui, S.; Lu, Q.; Qin, Y.; Guan, C.; Ren, X. Research on the Design and Multi-Dimensional Performance Enhancement of Ultra-High-Performance Concrete Based on Electric Arc Furnace Slag. *Constr. Build. Mater.* **2025**, *486*, 141943. [CrossRef]
48. Mohammed, A.J.; Hassan, M.S.; Al-Quraishi, H. Synergistic Effect of Nano-Silica, Steel Slag, and Waste Glass on the Microstructure, Electrical Resistivity, and Strength of Ultra-High-Performance Concrete. *Open Eng.* **2025**, *15*, 20240105. [CrossRef]

49. Kim, H.; Koh, T.; Pyo, S. Enhancing Flowability and Sustainability of Ultra High Performance Concrete Incorporating High Replacement Levels of Industrial Slags. *Constr. Build. Mater.* **2016**, *123*, 153–160. [CrossRef]
50. Juenger, M.C.G.; Snellings, R.; Bernal, S.A. Supplementary Cementitious Materials: New Sources, Characterization, and Performance Insights. *Cem. Concr. Res.* **2019**, *122*, 257–273. [CrossRef]
51. Nodehi, M.; Taghvaee, V.M. Alkali-Activated Materials and Geopolymer: A Review of Common Precursors and Activators Addressing Circular Economy. *Circ. Econ. Sustain.* **2022**, *2*, 165–196. [CrossRef]
52. Song, Q.; Guo, M.Z.; Wang, L.; Ling, T.C. Use of Steel Slag as Sustainable Construction Materials: A Review of Accelerated Carbonation Treatment. *Resour. Conserv. Recycl.* **2021**, *173*, 105740. [CrossRef]
53. Dhoble, Y.N.; Ahmed, S. Review on the Innovative Uses of Steel Slag for Waste Minimization. *J. Mater. Cycles Waste Manag.* **2018**, *20*, 1373–1382. [CrossRef]
54. Jiang, Y.; Ling, T.C.; Shi, C.; Pan, S.Y. Characteristics of Steel Slags and Their Use in Cement and Concrete—A Review. *Resour. Conserv. Recycl.* **2018**, *136*, 187–197. [CrossRef]
55. Wang, Q.; Wang, D.; Zhuang, S. The Soundness of Steel Slag with Different Free CaO and MgO Contents. *Constr. Build. Mater.* **2017**, *151*, 138–146. [CrossRef]
56. Wang, G.; Wang, Y.; Gao, Z. Use of Steel Slag as a Granular Material: Volume Expansion Prediction and Usability Criteria. *J. Hazard. Mater.* **2010**, *184*, 555–560. [CrossRef]
57. Martins, A.C.P.; Franco de Carvalho, J.M.; Costa, L.C.B.; Andrade, H.D.; de Melo, T.V.; Ribeiro, J.C.L.; Pedroti, L.G.; Peixoto, R.A.F. Steel Slags in Cement-Based Composites: An Ultimate Review on Characterization, Applications and Performance. *Constr. Build. Mater.* **2021**, *291*, 123265. [CrossRef]
58. Singh, S.K.; Vashistha, P.; Chandra, R.; Rai, A.K. Study on Leaching of Electric Arc Furnace (EAF) Slag for Its Sustainable Applications as Construction Material. *Process Saf. Environ. Prot.* **2021**, *148*, 1315–1326. [CrossRef]
59. Council of the European Union. Directive 2003/53/EC of the European Parliament and of the Council of 18 June 2003 Amending for the 26th Time Council Directive 76/769/EEC Relating to Restrictions on the Marketing and Use of Certain Dangerous Substances and Preparations (nonylphenol, nonylphenol ethoxylate and cement) (Text with EEA relevance). *Off. J. Eur. Union* **2003**, *178*, 24–27.
60. Council of the European Union. Regulation (EC) No 1907/2006 of the European Parliament and of the Council of 18 December 2006 Concerning the Registration, Evaluation, Authorisation and Restriction of Chemicals (REACH), Establishing a European Chemicals Agency, Amending Directive 1999/45/EC and Repealing Council Regulation (EEC) No 793/93 and Commission Regulation (EC) No 1488/94 as well as Council Directive 76/769/EEC and Commission Directives 91/155/EEC, 93/67/EEC, 93/105/EC and 2000/21/EC. *Off. J. Eur. Union* **2018**, *396*, 1–849.
61. *EN 12457-2:2002*; Characterisation of Waste—Leaching—Compliance Test for Leaching of Granular Waste Materials and Sludges—Part 2: One Stage Batch Test at a Liquid to Solid Ratio of 10 L/kg for Materials with Particle Size Below 4 mm (Without or With Size Reduction). European Committee for Standardization (CEN): Brussels, Belgium, 2002.
62. Council of the European Union. 2003/33/EC: Council Decision of 19 December 2002 Establishing Criteria and Procedures for the Acceptance of Waste at Landfills Pursuant to Article 16 of and Annex II to Directive 1999/31/EC. *Off. J. Eur. Union* **2002**, *11*, 27–49.
63. Council of the European Union. Council Directive 2013/59/Euratom of 5 December 2013 Laying down Basic Safety Standards for Protection against the Dangers Arising from Exposure to Ionising Radiation, and Repealing Directives 89/618/Euratom, 90/641/Euratom, 96/29/Euratom, 97/43/Euratom and 2003/122/Euratom. *Off. J. Eur. Union* **2014**, *13*, 1–73.
64. *EN 196-5:2011*; Methods of Testing Cement—Part 5: Pozzolanicity Test for Pozzolanic Cement. European Committee for Standardization (CEN): Brussels, Belgium, 2011.
65. Donatello, S.; Tyrer, M.; Cheeseman, C.R. Comparison of Test Methods to Assess Pozzolanic Activity. *Cem. Concr. Compos.* **2010**, *32*, 121–127. [CrossRef]
66. Kramar, S.; Ducman, V. Evaluation of Ash Pozzolanic Activity by Means of the Strength Activity Index Test, Frattini Test and DTA/TG Analysis. *Teh. Vjesn.* **2018**, *25*, 1746–1752. [CrossRef]
67. Mostafa, N.Y.; Brown, P.W. Heat of Hydration of High Reactive Pozzolans in Blended Cements: Isothermal Conduction Calorimetry. *Thermochim. Acta* **2005**, *435*, 162–167. [CrossRef]
68. Sun, X.; Liu, J.; Zhao, Y.; Zhao, J.; Li, Z.; Sun, Y.; Qiu, J.; Zheng, P. Mechanical Activation of Steel Slag to Prepare Supplementary Cementitious Materials: A Comparative Research Based on the Particle Size Distribution, Hydration, Toxicity Assessment and Carbon Dioxide Emission. *J. Build. Eng.* **2022**, *60*, 105200. [CrossRef]
69. Wu, X.; Roy, D.M.; Langton, C.A. Early Stage Hydration of Slag-Cement. *Cem. Concr. Res.* **1983**, *13*, 277–286. [CrossRef]
70. Ge, Z.; Wang, K.; Sandberg, P.J.; Ruiz, J.M. Characterization and Performance Prediction of Cement-Based Materials Using a Simple Isothermal Calorimeter. *J. Adv. Concr. Technol.* **2009**, *7*, 355–366. [CrossRef]
71. Amin, M.S.; El-Gamal, S.M.A.; Abo-El-Enein, S.A.; El-Hosiny, F.I.; Ramadan, M. Physico-Chemical Characteristics of Blended Cement Pastes Containing Electric Arc Furnace Slag with and without Silica Fume. *HBRC J.* **2015**, *11*, 321–327. [CrossRef]

72. Vàzquez Ramonich, E.; Barra, M. Reactivity and Expansion of Electric Arc Furnace Slag in Their Application in Construction. *Mater. Constr.* **2001**, *51*, 137–148. [CrossRef]
73. Roslan, N.H.; Ismail, M.; Khalid, N.H.A.; Muhammad, B. Properties of Concrete Containing Electric Arc Furnace Steel Slag and Steel Sludge. *J. Build. Eng.* **2020**, *28*, 101060. [CrossRef]
74. Qasrawi, H.; Shalabi, F.; Asi, I. Use of Low CaO Unprocessed Steel Slag in Concrete as Fine Aggregate. *Constr. Build. Mater.* **2009**, *23*, 1118–1125. [CrossRef]
75. Sedira, N. Novel Waste-Based Alkali-Activated Binders by Combining Mining and Other Mineral Waste. Ph.D. Thesis, Universidade da Beira Interior, Covilhã, Portugal, 2021.
76. Mo, L.; Zhang, F.; Deng, M.; Jin, F.; Al-Tabbaa, A.; Wang, A. Accelerated Carbonation and Performance of Concrete Made with Steel Slag as Binding Materials and Aggregates. *Cem. Concr. Compos.* **2017**, *83*, 138–145. [CrossRef]
77. Liu, Q.; Liu, J.; Qi, L. Effects of Temperature and Carbonation Curing on the Mechanical Properties of Steel Slag-Cement Binding Materials. *Constr. Build. Mater.* **2016**, *124*, 999–1006. [CrossRef]
78. De Ceukelaire, L.; Van Nieuwenburg, D. Accelerated Carbonation of a Blast-Furnace Cement Concrete. *Cem. Concr. Res.* **1993**, *23*, 442–452. [CrossRef]
79. Van Gerven, T.; Van Baelen, D.; Dutré, V.; Vandecasteele, C. Influence of Carbonation and Carbonation Methods on Leaching of Metals from Mortars. *Cem. Concr. Res.* **2004**, *34*, 149–156. [CrossRef]
80. *EN 197-1:2011*; Cement Composition, Specifications and Conformity Criteria for Common Cements. European Committee for Standardization (CEN): Brussels, Belgium, 2011.
81. *EN 933-1:2012*; Tests for Geometrical Properties of Aggregates—Part 1: Determination of Particle Size Distribution—Sieving Method. European Committee for Standardization (CEN): Brussels, Belgium, 2012.
82. *EN 1097-3:1998*; Tests for Mechanical and Physical Properties of Aggregates—Part 3: Determination of Loose Bulk Density and Voids. European Committee for Standardization (CEN): Brussels, Belgium, 1998.
83. *EN 1097-6:2022*; Tests for Mechanical and Physical Properties of Aggregates—Part 6: Determination of Particle Density and Water Absorption. European Committee for Standardization (CEN): Brussels, Belgium, 2022.
84. Roisnel, T.; Rodríguez-Carvajal, J. WinPLOTR: A Windows Tool for Powder Diffraction Pattern Analysis. *Mater. Sci. Forum* **2001**, *378–381*, 118–123. [CrossRef]
85. *EN 12457-4:2002*; Characterisation of Waste—Leaching—Compliance Test for Leaching of Granular Waste Materials and Sludges—Part 4: One Stage Batch Test at a Liquid to Solid Ratio of 10 L/kg for Materials with Particle Size below 10 mm (Without or With Size Reduction). European Committee for Standardization (CEN): Brussels, Belgium, 2002.
86. *ASTM C1702-17*; Standard Test Method for Measurement of Heat of Hydration of Hydraulic Cementitious Materials Using Isothermal Conduction Calorimetry. ASTM International: West Conshohocken, PA, USA, 2017.
87. *EN 12390-3:2019*; Testing Hardened Concrete—Part 3: Compressive Strength of Test Specimens. European Committee for Standardization (CEN): Brussels, Belgium, 2019.

Disclaimer/Publisher's Note: The statements, opinions and data contained in all publications are solely those of the individual author(s) and contributor(s) and not of MDPI and/or the editor(s). MDPI and/or the editor(s) disclaim responsibility for any injury to people or property resulting from any ideas, methods, instructions or products referred to in the content.